

Image registration and alignment of microscopy based images

Mikkel Rahbek
s072284



Kongens Lyngby 2013
IMM-M.Sc.-2013-64

Technical University of Denmark
Informatics and Mathematical Modelling
Building 321, DK-2800 Kongens Lyngby, Denmark
Phone +45 45253351, Fax +45 45882673
reception@imm.dtu.dk
www.imm.dtu.dk IMM-M.Sc.-2013-64

Summary (English)

The main goal of this project is to help the pathologist diagnose and stage breast cancer. This is done by combining information from different immunohistochemistry processes which each yields information regarding the cancer and can be combined into beneficial scores. This combination of information is called Virtual Double Staining and is developed at Visiopharm, a company in Denmark that specializes in Quantitative Digital Pathology. The combination is conducted by aligning serial sliced tissue samples that are stained with different antibodies.

An automatic Rigid registration method has been developed and modified to align the differently stained tissue samples. The registration method is based on frequency domain cross-correlation to estimate the rigid parameters between the tissue samples. The rotation parameter is estimated by transforming the images into polar representations. A weighting and a limitation is implemented to favour small steps in the rigid parameter estimation. The developed registration method is compared in a study with an existing registration algorithm at Visiopharm and a manual Point Based rigid registration conducted by four test subjects. A representative randomly selected dataset were extracted for the study. A study of the deformations fields showed that the developed method can not be determined significant different from the mean manual Point Based registration. A study with Mutual Information as the similarity measure showed that 92% of the registrations were better than the existing algorithm in Visiopharm's software.

Summary (Danish)

Hovedformålet med dette projekt er at hjælpe patologerne diagnosticere og stadié inddøle brystkræft. Dette gøres ved at kombinere informationer fra forskellige former for immunhistokemi processer. De forskellige immunhistokemi processer bidrager hver med oplysninger omkring den potentielle kræft lokaliseret i vævet. Disse oplysninger kan kombineres til scorer der bruges til diagnosticering og stadié inddeling. Denne form for kombineret af information kaldes Virtual Double Staining og er udviklet hos Visiopharm, et selskab i Danmark, der har specialiseret sig i kvantitativt digital patologi. Virtuel Double Staining udføres ved at registrere serielle skåret vævsprøver, der er farvet med forskellige antistoffer.

Til at kombinere vævsprøverne er der blevet udviklet og modificeret en automatisk rigid registrering til at estimere de rigide parameterne mellem vævsprøverne. Registrerings metoden er baseret på krydkorrelation i frekvensdomænet til at estimere translations parameteren. Rotations parameteren estimeres ved at omdanne billederne til polære repræsentationer. Yderligere er der implementeret en vægtning og en begrænsning for at favorisere små skridt i den rigide registrering. Metoden er sammenlignet, i en ad hoc statistisk undersøgelse, med den eksisterende registrerings algoritme i Visiopharm's software og en manuel Punkt Baseret rigid registrering udført af fire forsøgspersoner. Et repræsentativt tilfældig udvalgt data sæt blev brugt i undersøgelsen. Studiet viste, at den udviklede metoder ikke er signifikant forskellig fra den gennemsnitlige manuelle Punkt Baseret registrering ved at sammenligne deformationsfelte. Ved brug af similaritetsmålet Mutual Information viste en ad hoc statistisk undersøgelse, at 92 % af registreringerne var bedre end registreringerne med den eksisterende algoritme i Visiopharm's software.

Preface

This thesis was prepared at the department of Informatics and Mathematical Modelling at the Technical University of Denmark in fulfilment of the requirements for acquiring an M.Sc. in Biomedical engineering. The extend of this thesis is equivalent to 35 ECTS points.

This thesis was prepared in collaboration with Visiopharm a company that specializes in Quantitative Digital Pathology.

The project supervisors are Rasmus Larsen, Professor in Image Analysis, and Knut Conradsen, Professor in Image Analysis. The external supervisor is Michael Friis Lippert, IVD project manager at Visiopharm.

This thesis deals with image registration of microscopic image. The focus of the project is to generate a rigid registration model that can align serial sliced tissue samples of breast cancer biopsies. The tissue is aligned to combine information from different immunohistochemistry processes. This procedure is called Virtual Double Staining.

The thesis consists of a theory section followed by an introduction to the concept of Virtual Double Staining. The image registration method is then described and its results are presented. The results are discussed followed by a conclusion and a perspective.

The data provided for this project consists of tissue samples from breast cancer patients and is handled with care. The data is anonymized with no trace back to individual patients.

Lyngby, 15-July-2013

A handwritten signature in blue ink, appearing to read "Mikkel Rahbek".

Mikkel Rahbek
s072284

Acknowledgements

I would like to thank the following people for support and assistance in this project.

I thank my main supervisors Rasmus Larsen and Knut Conradsen for great support at the weekly supervision meetings.

A thanks to Visiopharm for great cooperation during the project and for providing the data.

A special thanks to Michael Friis Lippert at Visiopharm for always having time to spare for guidance.

Thanks to the four test subject for their contribution to the statistical analysis.

Nomenclature

Symbols	Meaning
t	Translation parameter
\mathbf{R}	Rotation parameter
θ	Angle input for the rotation parameter
t_r	Translation parameter to calculate rotation
I_1	Image for registration
I_2	Image for registration
I_p	Phantom for registration
F	Fourier transform
F^{-1}	Inverse Fourier Transform
Y	Deformation field
$C(u)$	2D IFFT cross-correlation
θ_p	Angle of wheel spoke in polar coordinate system
ρ	Sampling along wheel spoke in polar coordinate system
λ	Wave length
γ	Spatial aspect ratio
k	denotes annotation point
i	Pixel
j	Core number in subset
n	Test person
α	Level of significance

Abbreviation	Meaning
VDS	Virtual double staining
IHC	Immunohistochemistry
PHH3	Phosphohistone H3
PCK	Pancytokeratin
CK	Cytokeratin
ER	Estrogen receptor
ER-PCK	Estrogen receptor Pancytokeratin
CT	Computer Tomography
MRI	Magnetic Resonance Imaging
MI	Mutual Information
SSD	Sum of Squared Difference
PDF	Probability Density Function
TMA	Tissue Micro Array
.tiff	Tagged Image File Formats
FT	Fourier Transform
FFT	Fast Fourier Transform
IFT	Inverse Fourier Transform
iFFT	Inverse Fast Fourier Transform
R	Red channel in the RGB images
G	Green channel in the RGB images
B	Blue channel in the RGB images
FB	Fast Fourier Transform Based rigid registration method
PB	Point Based rigid registration method

Software

MATLAB	High-level technical computing software
--------	---

Contents

Summary (English)	i
Summary (Danish)	iii
Preface	v
Acknowledgements	vii
Nomenclature	ix
1 Introduction	1
2 Theory	5
2.1 Mamma cancer	5
2.2 Immunohistochemistry	6
2.3 Staining types	7
2.4 Rigid registration	9
2.5 Similarity measures	10
2.5.1 Mutual Information	11
2.6 Sum of Squared Difference	12
3 Virtual Double Staining	13
3.1 Scores and ratios	17
4 Methodology	19
4.1 Dataset	19
4.2 Extraction of data	20
4.3 Rigid registration	22
4.4 Fast Fourier Transform based rigid registration	22

4.4.1	Translation	23
4.5	Implementation of FFT based translation	23
4.5.1	Rotation	26
4.5.2	Polar representation	27
4.6	Iterative rigid registration process	30
4.7	Weighting and limitation	32
4.8	Zeropadding	41
4.9	Phantom	43
4.10	Pre-processing tests	44
4.10.1	Gabor filter	45
4.10.2	Chromaticity	50
4.11	Manual registration	53
4.11.1	Point based rigid registration	55
4.12	Statistical analysis setup	56
4.13	Registration GUI	58
4.14	Overview of the Fast Fourier Transform Based method	59
5	Results	61
5.1	Phantom	61
5.2	Dataset	62
5.3	Manual placement of annotation points	68
5.4	Statistical analysis of extracted dataset	69
5.5	Statistical analysis of the deformation field	69
5.6	Statistical analysis of similarity measure	74
5.7	Rotation study	85
6	Discussion	87
6.1	Phantom	87
6.2	Manual Point Based registration	88
6.3	Statistical analysis	88
6.4	Rotational Study	91
6.5	Computation time	91
6.6	Method	92
6.7	Pre-processing	93
6.8	Similarity measure	94
7	Conclusion	97
A	Computer specs.	99
B	Registration GUI demo	101
C	Full dataset comparison	105
D	CD	107

Bibliography	109
---------------------	------------

CHAPTER 1

Introduction

Cancer caused approximately 7.6 million deaths world wide in 2008 which is about 13% of all deaths. This disturbingly high number insinuates why cancer is also one of the largest fields of research in medical science. The development of new ways to diagnose, investigate, alleviate and cure the disease is very essential to help the large population that is affected by cancer. There are over 200 different types of cancer variations and the occurrence differs between genders. In this project the focus area is to help diagnose and stage breast cancer to determine the course of individual treatment.

The main goal is to help the pathologist perform a sufficient analysis of biopsies from breast carcinomas. After the extraction the biopsies are moulded in paraffin and sliced before they are marked with different types of antibodies. This is to emphasize for instance epithelial cells, carcinomas or nuclei about to undergo cell division. These procedures are done separately to serial sliced sections of tissue and the goal of this project is to combine the information from each of the staining procedures and thereby improve the pathologist's possibility of making an adequate diagnosis or prognosis. This procedure is what Visiopharm denotes as Virtual Double Staining (VDS). Visiopharm is a company that specializes in Quantitative Digital Pathology.

The biopsy is sliced serially and stained with two or three desired antibodies. The differently stained slices of tissues are then placed under the microscope

and digitalized as virtual slides. Two virtual serial sliced microscopy images are visualized in figure 1.1.

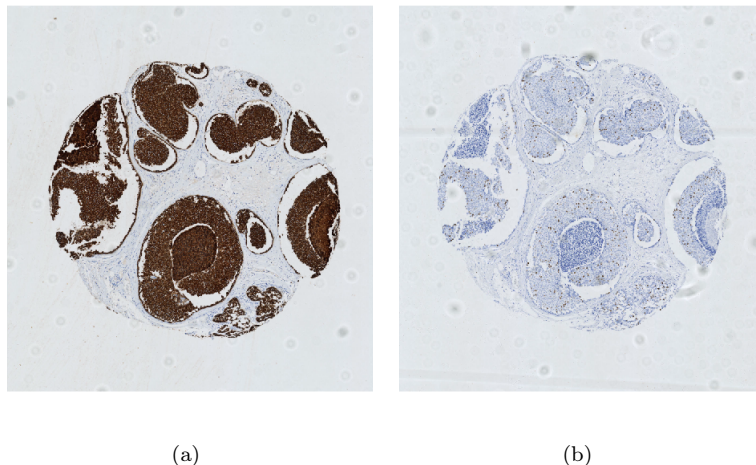


Figure 1.1: Microscopy images of a serial sliced TMA core. a) Tissue stained with PCK which is a marker for epithelial cells. b) Tissue stained with KI-67 which is a cell nucleus marker that can determine the amount of cellular division.

The desired result is to combine the result from both of the stained microscopic images in figure 1.1. The task of combining the image information is conducted using rigid image registration consisting of a translation and a rotation of the images.

An alternative method of combining information from two types of staining is multiple staining of the same tissue slice. But this procedure is very advanced and is performed manually which induces a larger human error since the procedure is unfamiliar to many lab technicians and is complicated to perform.

Problem statement

The project definition was to implement a rigid registration for differently stained serial sections on Tissue Micro Array microscopy. The registration results obtained are to be compared with the results of an existing algorithm in Visiopharm's software.

The deposition of the report

The report consists of a theory section containing basic descriptions for prior enlightenment to the project. The theory section is followed by a methodology section describing the developed, used and modified methods to conduct and evaluate the rigid registration results. The results of the study is then presented together with a discussion of the result. The results of the project is then summarized in a final conclusion together with future perspectives.

CHAPTER 2

Theory

This chapter contains an introduction of mamma cancer and a description of immunohistochemistry together with different types of antibodies used for staining. The basis theory of rigid registration is presented followed by a description of two similarity measures.

2.1 Mamma cancer

Mamma cancer is the most common invasive cancer in women. There are approximately 4700 new cases pr. year in Denmark and approximately 12.7 million women were diagnosed with mamma cancer in 2008 [4]. These statistics lead to the important innovative work conducted in this medical area. Along with curing the disease it is desired to diagnose mamma cancer as early as possible and develop individual treatment plans. The treatment plans are individual since different types of mamma cancer need different treatment plans.

The protocol to detect and diagnose mamma cancer is divided into three steps. The first is a mammography where low energy x-rays are used to screen and diagnose the mamma cancer. The second is palpation which is a physical

examination by a physician to determine the size, shape and placement of the area of interest. The last step to make a final diagnose of a possible malignant tumor is done with a biopsy. The biopsy is submitted to the pathologist who can determine if the tumor is malignant, the stage and various other features which affects the prognosis of the patient. For the pathologist to examine the tissue, microscopy images of the biopsy are generated after the tissue is processed with different immunohistochemistry (IHC) procedures. These processes yields different information regarding type and aggressiveness of the tumor. The different immunohistochemistry processes used in this project are described in section 2.3.

2.2 Immunohistochemistry

Immunohistochemistry is used in diagnostics of diseases, biomedical research and many other medical aspects. IHC is among others used by physicians to determine if a tissue biopsy is benign or malignant, cell division, the stage of the cancer and the primary origin of the cancer. These processes provides highly usable information regarding the prognosis and desired treatment of the cancer.

The IHC process uses labelled antibodies to bind to specific antigens. The process is displayed in figure 2.1 where the chosen antibody connects with the antigen in the tissue. This example is shown for direct IHC, the indirect method uses a primary rapid unlabelled antibody to connect with the antigen and then a secondary labelled antibody to connect with the primary antibody.

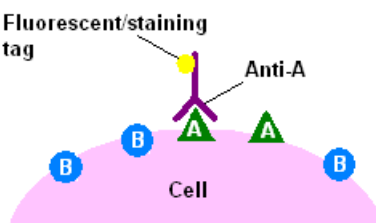


Figure 2.1: Illustration of an Immunohistochemical staining process [2].

There are a large amount of different antibodies that are used in medical practise and biomedical research. The staining processes used on the VDS dataset acquired for this project, are described in the following section.

2.3 Staining types

The different antibodies used for staining in this project are listed below. They each contribute with different information regarding the possible disease located in the tissue of interest.

Ki-67 MIB-1

Antigen Ki-67 is a protein that can be used as a cellular marker to determine cell division, where a mother cell divides into two daughter cells. Ki-67 is absent in resting cells but present during all the active phases of the cell division cycle, namely G1, S, G2 and mitosis. The Ki-67 protein is identified by the monoclonal antibody Ki-67 MIB-1 and is stated as Ki-67 positive cells. The Ki-67 positive tumor marker is applied to determine the growth fraction of a cell population and then used in the evaluation of the clinical course of various cancer types. An example of the Ki-67 staining is displayed in figure 2.2(a).

Phosphohistone H3

Phosphohistone H3 (PHH3) is a histone protein that is a general component in chromatin. The histone protein is only phosphorylated at Serine-10 and Serine-28 during mitosis. At the other stages of the cell cycle no phosphorylation occurs. An antibody is generated to recognise the Phosphohistone H3 and this makes it a good mitosis marker. The PHH3 marker has a strong prognostic value in early invasive lymph node-negative breast cancer [8]. An example of the PHH3 staining is displayed in figure 2.2(b).

Erb-B2

The erb-B2 is a receptor of tyrosine kinases and is implicated in physiological processes concerning growth and development. The erb-B2 receptor is seen to be over expressed in cancers that are aggressive, likely to metastasize and often have a poor clinical outcome. The alterations in the erb-B2 can be seen in e.g. breast tumors and ovarian tumors [7]. An example of the erb-B2 staining is displayed in figure 2.2(c).

Pancytokeratin

Pancytokeratin (PCK) is a staining type used to detect carcinomas in the epithelial tissue. It is a broadly reactive reagent that recognize almost all epithelial tissue. It helps distinguish between healthy tissue and malignant tissue. An example of the Pancytokeratin staining is displayed in figure 2.2(d).

Cytokeratin AE1-AE3

Cytokeratin (CK) AE1-AE3 is a mixture of two different anti-cytokeratin monoclonal antibodies. Each of the antibodies detects different keratins of high and low molecular weight, giving a broad reactivity of cytokeratins. The AE1-AE3 does not detect as many cytokeratins as a pancytokeratin. An example of the cytokeratin AE-AE3 staining is displayed in figure 2.2(e).

Estrogen receptor

Estrogen receptor (ER) is a group of proteins that are located inside the cells. It is activated by the hormone estrogen and is found linked to 70 % of all cases with breast cancer. The increase of Estrogen receptor is referred to as ER-positive and affects the clinical course of the cancer type. An example of the Estrogen receptor staining is displayed in figure 2.2(f).

Estrogen receptor Pancytokeratin

A combination of the Estrogen receptor and the Pancytokeratin described above. An example of the Estrogen receptor Pancytokeratin staining is displayed in figure 2.2(g).

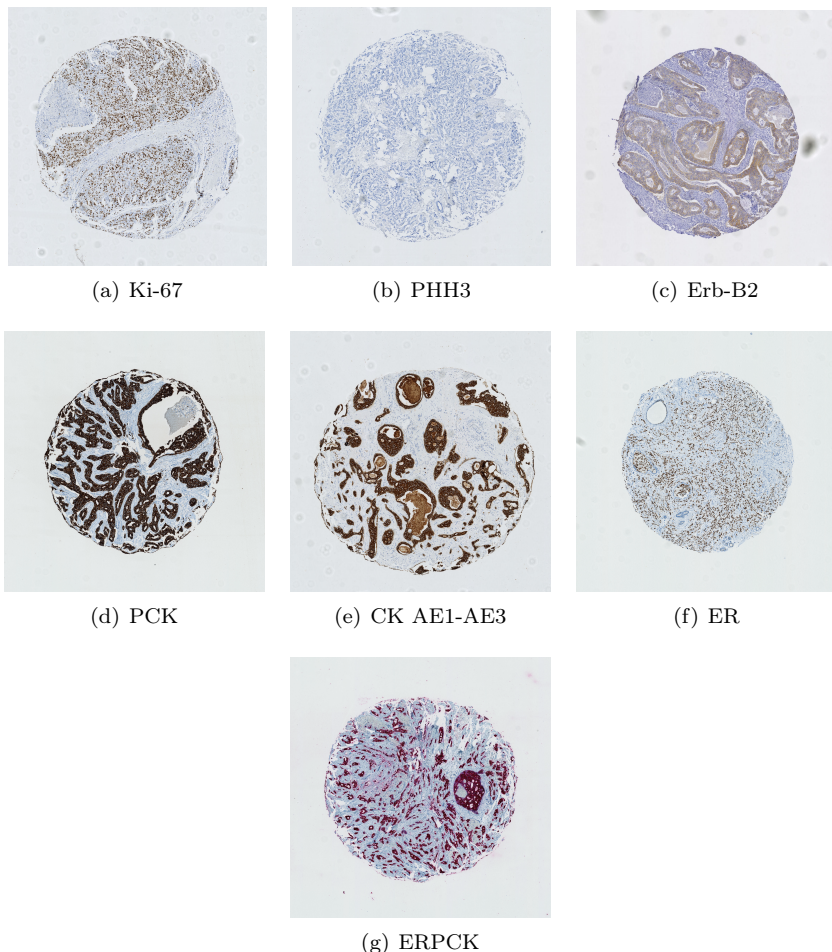


Figure 2.2: Overview of the different staining procedures applied on the dataset acquired for this project. The individual stains are listed below the images.

2.4 Rigid registration

The registration conducted in this project is rigid registration, the basic theory of rigid registration is briefly presented in this section.

Rigid registration is constrained to a translation parameter t and a rotation parameter \mathbf{R} . All rigid registration is performed in 2D for this project. The

estimation of the translation parameter and the rotation parameter can be conducted in many different ways. This thesis deals with developing an automatic, robust and computationally efficient method for calculating the optimal rigid transformation parameters.

The rotation is customarily represented by an orthogonal matrix \mathbf{R} , i.e., $\mathbf{R}^T\mathbf{R} = \mathbf{I}$. This orthogonal matrix describes both the rotation and the rotation-reflections. The rotation-reflections is excluded by setting $\det(\mathbf{R}) = 1$. The rigid transformation can then be described as the following.

$$y(x; \mathbf{R}, t) = \mathbf{R}x + t \quad (2.1)$$

Where t describes the translation and \mathbf{R} describes the rotation. \mathbf{R} is given as the following for the rotation in 2D.

$$\mathbf{R} = \begin{pmatrix} \cos(\theta) & -\sin(\theta) \\ \sin(\theta) & \cos(\theta) \end{pmatrix} \quad (2.2)$$

The registration methods developed and modified to estimate t and \mathbf{R} in this project is described in Chapter 4.

2.5 Similarity measures

The validation of image registration is often difficult to execute since the ground truth is nearly impossible to find. Intensity based measures are one approach to quantify how good a registration of two images are.

The data provided for registration in this project has the characteristics of two different modalities since different staining procedures provides different images characteristics as visualized in the previous figure 2.2. The PCK marks the epithelial tissue brown and nuclear blue opposed to Ki-67 that only marks the nuclear in different scales of brown. This suggests the use of Mutual Information (MI) as a similarity measure since it is known to be favourable when registering different modalities such as MRI with CT. The Mutual Information is not used as a part of the registration method but applied on the final result from the registration to be able to compare with other results.

The calculation of MI is presented in the following section. Other similarity measures such as Sum of Squared Difference (SSD) could also be used but is

not as favourable as MI. The prior considerations regarding the use of SSD as a similarity measure is presented in section 2.6

2.5.1 Mutual Information

The measure Mutual information is calculated as the following [5]

First the normalized joint histogram is calculated for an image A as

$$\text{PDF}[j, k] = \frac{\text{HIST}[j, k]}{\sum_{j,k} \text{HIST}[j, k]} \quad (2.3)$$

Where j and k are pixel coordinates. A and B' are two different images, where the Joint Entropy $H(A, B')$ is calculated as

$$H(A, B') = - \sum_{j,k} \text{PDF}[j, k] \log \text{PDF}[j, k] \quad (2.4)$$

The marginal entropy is also taken into account and is calculated for $H(A)$ and $H(B')$

$$H(A) = - \sum_j \left(\sum_k \text{PDF}[j, k] \log \sum_j \text{PDF}[j, l] \right) \quad (2.5)$$

$$H(B') = - \sum_j \left(\sum_i \text{PDF}[i, k] \log \sum_j \text{PDF}[j, k] \right) \quad (2.6)$$

the Mutual information can then be calculated as

$$\text{MI}(A, B') = H(A) + H(B') - H(A, B') \quad (2.7)$$

The Mutual Information is used as the similarity measure. Other versions of MI, such as Normalized Mutual Informations, are known but not used for this project.

2.6 Sum of Squared Difference

Sum of Squared Difference is another similarity measure used to evaluate the difference between two images or used to align images. Sum of Squared Difference is for instance used to register MR images from two scans of the same person to compare tumor size over time etc. The best result is often obtained if the images to be aligned are of the same modality. The SSD is given as the following

$$\text{SSD} = \frac{1}{N} \sum_i^N |A(i) - B'(i)|^2 \quad \forall i \in A \cup B' \quad (2.8)$$

Here A and B are images and i is pixels. The SSD is used as a measure to evaluate the rigid registration algorithm when applied to the phantom created in section 4.9.

As discussed in the previous section 2.5, the cores are applied with different staining protocols emphasizing different features in the tissue samples. This creates different intensities in the images and SSD is therefore not used in the evaluation of the result of the rigid registration of tissue samples.

CHAPTER 3

Virtual Double Staining

The information extracted from different Immunohistochemistry (IHC) processes described in section 2.2 provides valuable knowledge about the tissue of interest. This information is what Virtual Double Staining is developed to combine. The combination of information from different antibodies yields easier scores related to diagnostics of the ROI and possibly new score combinations. The VDS protocol is described in this section giving an introduction to the major steps in the process. The data provided was collected by a second party prior to the project initiation. A short description of a typical tissue preparation[3] is described in the following section.

Tissue preparation

A series of steps need to be completed before scanning the tissue sample with the microscope. First the tissue of interest is extracted with e.g a scalpel biopsy or needle biopsy seen in figure 3.1. The tissue samples are then fixated immediately to prevent the breakdown of cellular structures etc. The fixation method is determined by the target antigen to yield the best result. The most common fixative is formaldehyde. The fixated large biopsy is then embedded in paraffin to preserve the structures.

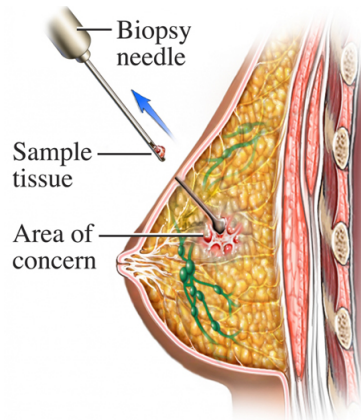


Figure 3.1: Illustration of a needle biopsy, taken to study the tissue of concern. A larger area can also be removed with a scalpel [1].

Core extraction and slicing

After the paraffin embedding a series of Tissue Micro Array (TMA) cores are extracted and inserted in to a new paraffin block containing many different tissue samples. This procedure is visualized as a flow diagram in figure 3.2. After the paraffin embedding and core extraction, the TMA tissue samples are ready for serial sectioning.

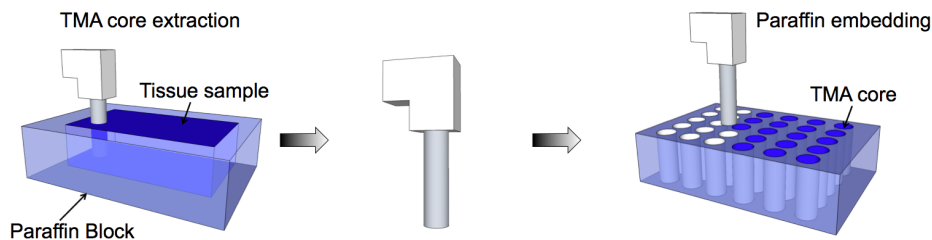


Figure 3.2: Flow diagram of the Paraffin embedding and TMA core extraction. The large tissue sample is embedded in paraffin, prior to the core extraction. Then various tissue samples are extracted as cores to be placed as a part of a Tissue Micro Array. The paraffin embedding makes it possible to slice the tissue samples in micrometer thin slices.

The serial slicing of the sections is one of the main parts in VDS, here sections of $4\text{-}5 \mu\text{m}$ are sliced with a microtome and the serial slices are carefully ordered in slice numbers. This is important because we can then assume that two serial sliced tissue samples have the same major characteristics and are therefore able to be registered to each other. The microtome is estimated to loose around $1 \mu\text{m}$ in the slicing process. The slides are added on to glass slides that are coated with adhesives.

The glass slides with serial sliced tissue samples are numbered. The selected staining procedures are then applied to the sliced tissue samples and subsequently aligned.

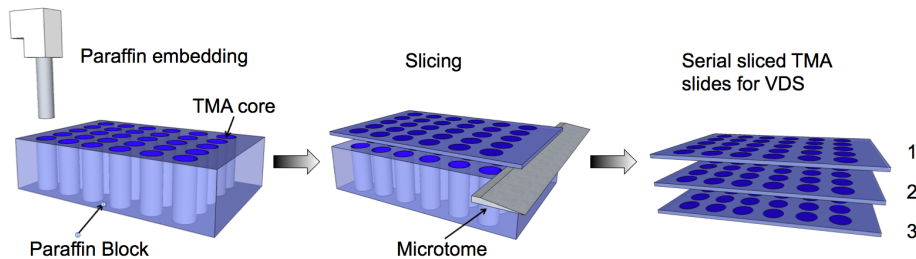


Figure 3.3: Flow diagram of the Paraffin embedding and slicing process. The tissue samples are embedded in the paraffin block prior to the slicing. The paraffin embedding makes it possible to slice the tissue samples in micron thin slices. The slicing is conducted with a microtome which is set for a desired thickness. The slides are approximately $4\text{-}5 \mu\text{m}$ thin after slicing. Three adjacent slides are cut from the paraffin block. The TMA slides are then placed on glass slides before initializing the staining process.

Staining and registration of VDS

To begin the staining process with the antibodies, the paraffin needs to be completely removed, which is done with a series of chemical processes. Then the selected antibody is applied to mark the antigen. A counter stain can be applied after the primary stain to provide contrast. The different types of staining are described previously in section 2.2. The stained TMA slides are then sealed with a cover glass to preserve the tissue.

The stained tissues slides are now inserted into a virtual slide scanner that

generates virtual slides that are saved for further image registration and image processing. The three steps of slicing, staining and generating virtual slides are displayed in the top row of the flow diagram in figure 3.4. Here the serial sliced sections are stained with three different antibodies. Number one is stained with Ki-67, number two is stained with PCK and number 3 is stained with PHH3. The antibody that is preferable to be registered to both Ki-67 and PHH3 is optimally applied to the slide in the middle. This results in the best possible fit and suits the assumption that the tissues share major characteristics. The upper right illustration displays the virtual slides generated from slide number 1 and 2.

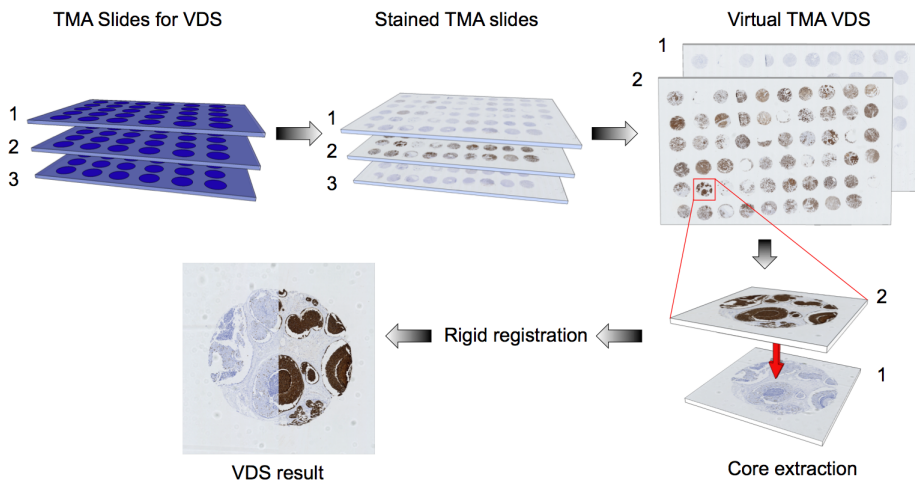


Figure 3.4: Flow diagram of the staining process, extraction of virtual core and rigid registration. The serial sliced sections are individually stained with different antibodies. The middle slide is stained with the desired antibody to combine with the other two antibodies. Slide 1: Stained with Ki-67. Slide 2: Stained with PCK. Slide 3: Stained with PHH3. Slide 1 and 2 are scanned and saved as virtual slides and the core with the red square is extracted for registration. Then the rigid registration is calculated and applied resulting in the combined information as an overlay in the last step in the flow diagram.

The same core but differently stained is then extracted from both of the virtual TMA slides. The extracted core is marked with a red square in the upper right of the flow diagram in figure 3.4. Then the rigid registration parameters are estimated and applied. The result is visualized as an overlay of

the Ki-67 and PCK stained core. After applying image analysis this result can be used for calculating a number of scores and ratios that help the pathologist to analyse the tissue. The different scores and their use is briefly described in the next section.

3.1 Scores and ratios

The final result of the Virtual Double staining can be used to generate scores to determine various informations regarding the cancer. Some of the relevant score for the antibodies used for these VDS data are:

- Estrogen receptor (ER)

$$\text{Positive ratio} = \frac{\text{Positive nuclei}}{\text{Total number of nuclei}}$$

H-score from 0-300

Each nucleus is given a score from 0 to +3 which depict the scale of how positive the nucleus is. 0 is negative. +1 is slightly. +2 is medium. +3 is total. And the positive ratio is the calculated.

- Ki-67

$$\text{Positive ratio} = \frac{\text{Positive nuclei}}{\text{Total number of nuclei}}$$

- PHH3

$$\text{Positive count} = \frac{\text{Positive count}}{\text{Area of tumor tissue}}$$

These scores and ratios each give the pathologist information regarding the tumor. For instance the Ki-67 stains nuclears in the proliferation stage and therefore yields a number of how much cell divisions occurring in the tissue. The positive ratio calculated with the Ki-67 antibody gives the pathologist an idea of the aggressiveness of the tumor. This information influences the treatment planning of the patient. The Ki-67 positive ratio can be divided into 3 categories with different outcomes listed in table 3.1.

Table 3.1: Ki-67 positive ratio

Positive ratio [%]	0 – 1%	1 – 10%	> 10%
Indication	Negative	Borderline	Positive

The different categories indicates the extent of the disease. The outcome of the Ki-67 contributes to the prognosis and treatment planning of the patient.

CHAPTER 4

Methodology

This chapter contains a description of the developed and modified methods used in this project. The dataset provided for the project is described. Furthermore it contains a description of a manual rigid registration method to compare the registration result. An adapted statistical analysis is created to compare the results from the developed registration method, the manual registration and the existing registration algorithm at Visiopharm.

The method behind the rigid registration algorithm at Visiopharm is reserved to their knowledge only and is therefore not described in this report.

4.1 Dataset

The dataset is provided by Visiopharm and is generated according to the VDS protocol described in section 3. The data is generated by qualified lab technicians in collaboration with a pathologist and Visiopharm. The dataset consist of 6 batches from the pathology department at Aalborg University Hospital. The dataset can be listed as the following:

- 102 tissue samples from Aalborg, stained with AE1-AE3, erb-B2 and

MIB.

- 19 tissue samples from Aalborg, stained with AE-AE3, Ki-67 and PHH3.
- 59 tissue samples from Aalborg, stained with PCK, ER and ER-PCK.
- 59 tissue samples from Aalborg, stained with PCK, ER and ER-PCK.
- 59 tissue samples from Aalborg, stained with PCK, Ki-67 and PHH3.
- 59 tissue samples from Aalborg, stained with PCK, Ki-67 and PHH3.

All the data is provided as virtual slides and the cores extracted are in .tiff image file format. The dataset consists of 357 tissue samples that are serial sliced 3 times and stained differently, leaving a total of $3 \times 357 = 1071$ cores.

4.2 Extraction of data

The data is presented in large virtual TMA slides containing all cores in one image. The extraction of the cores is conducted with Visiopharm's software and is denoted de-arraying. The de-arraying is done semi-automatic. A visualization of the user interface for the de-arraying is displayed in figure 4.1.

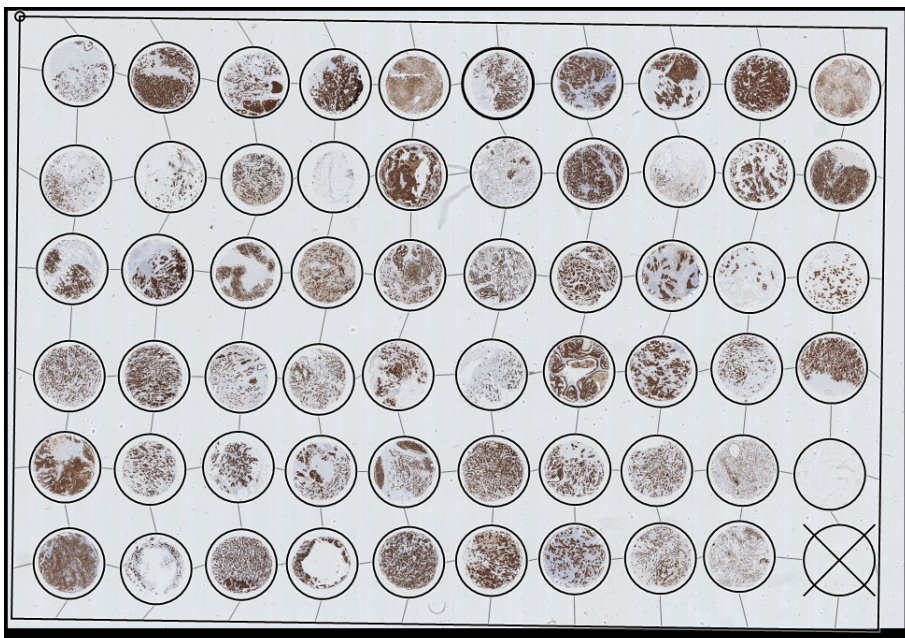


Figure 4.1: De-arraying interface in Visiopharm's software.

The de-arraying protocol is very important for the registration of the cores. The TMA cores location in the image extracted from the large virtual TMA slide has a large influence on the estimation of the relation in rigid registration parameters. The procedure of extracting the cores are described in the following.

A grid of circles are placed across the cores to denote the areas where the cores are located within. An automatic detection of the cores can then be initialized to fit the circles to the cores. After the automatic core detection, a manual inspection of the circles is performed before the cores are extracted. The process is then repeated with the corresponding serial sliced virtual TMA slide with a different staining. The extracted cores are then used as input in the automatic rigid registration algorithm.

The fit of the circles in the de-arraying process has a large influence on the difficulty of the registration task. To create the highest possibility of conducting a sufficient rigid registration, a set of guidelines are made about the de-arraying output.

- The cores have to be centered within the extraction circle.

- The virtual TMA slide is manually inspected to detect possible 180 degree rotation of the whole TMA slide when performing the scan or if the TMA slide is inverted.

These guidelines have to be followed, for the extracted cores to qualify as a proper input for the rigid registration algorithm. It can then be assumed that the translations are fairly small and rotations of 180 degrees are most unlikely.

4.3 Rigid registration

There are many different ways of performing rigid registration. They can among others be divided into two groups, user dependent and automatic methods. The user dependent methods will always depend on the operator in terms of experience, work load, time of day and many other things. The automatic methods are user independent and can have the ability to reproduce results regardless of the operator.

This project focuses on the development of an automatic, robust and computationally efficient rigid registration method for microscopy based images. The rigid registration is conducted with a modified Fast Fourier Transform based (FB) registration method which is described in the following sections.

4.4 Fast Fourier Transform based rigid registration

The method implemented for in this project is based on Fast Fourier Transform (FFT). The FFT approach is known to be computationally efficient and relative robust. The FFT is issued in both the estimation of the translation parameter and the rotation parameter. The first step described is the translation.

4.4.1 Translation

The translation is calculated with the FFT and is described and derived based on [9]. If two images denoted I_1 and I_2 that are assumed to be related with an unknown relation in translation (t) between them, their relation can be written as the following.

$$I_2(x) = I_1(x + t) \quad (4.1)$$

By using 2D cross-correlation t can be estimated. If it is assumed that the two images are of finite energy this can be done with the function $C(u)$ given as the following.

$$C(u) \triangleq I_1(u) \star I_2(-u) = \int_{\mathcal{R}^2} I_1(x) I_2(x + u) dx \quad (4.2)$$

here $\mathbf{u} = [u, v]^T \in \mathcal{R}^2$ as $\hat{t} = \arg_u \max\{C(u)\}$. By using the convolution theorem of Fourier Transform (FT) [6], C can be written as

$$C(u) = F^{-1} \left\{ \widehat{I}_1(K) \widehat{I}_2^*(K) \right\} \quad (4.3)$$

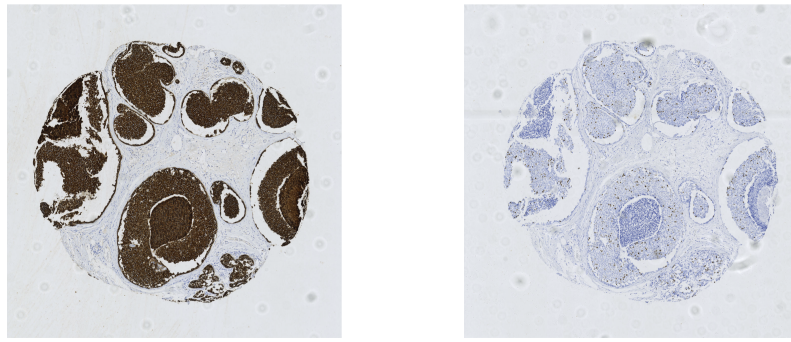
Here F^{-1} is the inverse Fourier Transform (iFT) and $*$ is the complex conjugated. The maximum peak of $C(u)$ now indicates the related translation between I_1 and I_2 .

This describes the main theory of the frequency domain correlation-based translation estimation. In the algorithm the forward and inverse FT are conducted using FFT and Inverse Fast Fourier Transform (IFFT).

4.5 Implementation of FFT based translation

The FB method for estimating the relation in translation (t) between two images I_1 and I_2 is implemented in MATLAB. The implemented algorithm is then tested on the dataset described in section 4.1 and further on a subset described in 5.2.

The first step to estimate the translation in the FB rigid registration method is to define the input consisting of the two differently stained serial sliced tissue samples for VDS registration. An example of a virtual core that is serial sliced and stain differently is visualized in figure 4.2.



(a) TMA core, I_1 , stained with PCK

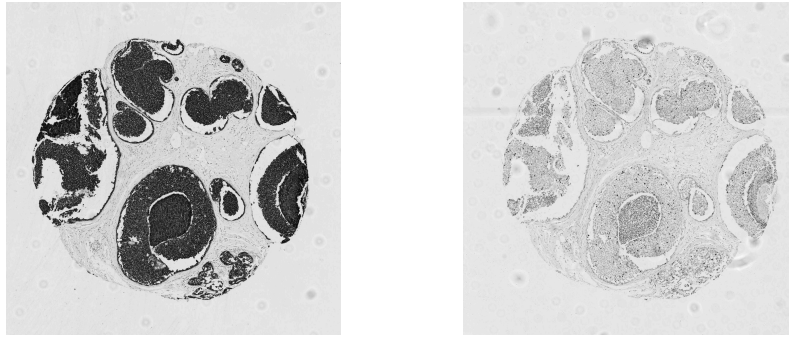
(b) TMA core, I_2 , stained with Ki-67

Figure 4.2: Two tissue samples that are serial sliced as described in chapter 3. The slices are stained with two different antibodies to yield different information about the tissue.

The dataset consists of microscopy RGB images. Before they are used as input in the algorithm they are transformed into grey-scale images as the following

$$I_{gray-scale}(i) = 0.2989 \cdot R(i) + 0.5870 \cdot G(i) + 0.1140 \cdot B(i) \quad (4.4)$$

where i is pixels and $I_{gray-scale}$ is the gray scale image. The results from the grey-scale transformations are displayed in figure 4.3.



(a) TMA core, I_1 , stained with PCK (b) TMA core, I_2 , stained with Ki-67

Figure 4.3: The grey scale images of the two tissue samples in figure 4.2. The tissue samples are serial sliced as described in chapter 3. the slices are stained with two different antibodies to yield different information about the tissue.

The two grey scale images can now be used as input in the algorithm to estimate the relation in the translation t between I_1 and I_2 . The 2D Fast Fourier Transform is calculated for both I_1 and I_2 with the command FFT2. The 2D Inverse Fourier Transform is then calculated on the two 2D FT that have been multiplied where one is the complex conjugated. This yields a 2D IFFT that reflects the relation in translation between the two images.

The maximum of the 2D Inverse Fourier Transform indicates the estimated translation. The 2D Inverse Fourier Transform between the images displayed in figure 4.3 is visualized in figure 4.4. Here the maximum, indicated by a green sphere, depicts the translation t in the x and y directions. The IFFT result is not visualized as fftshifted, since it is easier to locate the direction of the translation t in the none fftshifted plot.

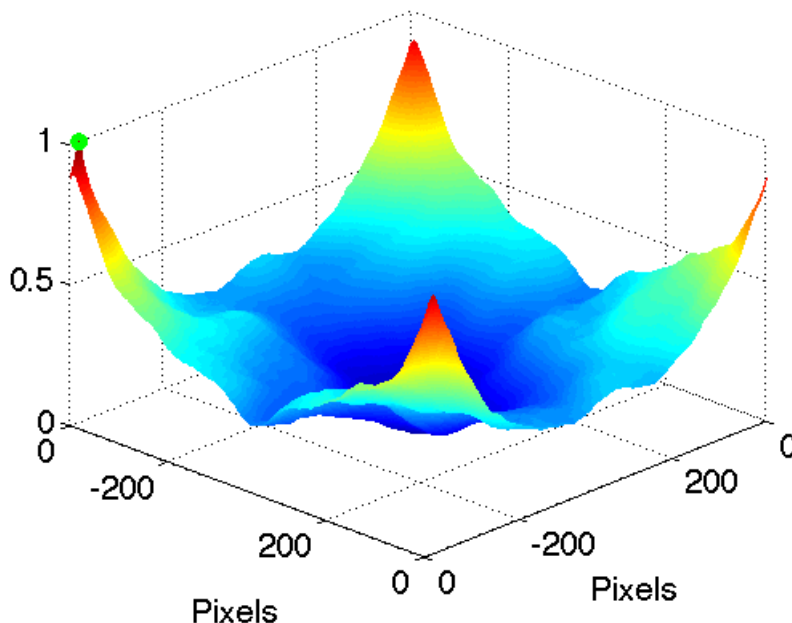


Figure 4.4: 2D Inverse Fourier Transform of the serial slice selected core in figure 4.3. The green sphere indicates the maximum and depicts the relation in translation between the two images. For these two images the relation in translation is estimated to -13 pixels in the x direction and -8 in the y direction.

In this particular case the relation in translation is estimated to -13 pixels in the x direction and -8 in the y direction. The estimated translation can then be applied to the images and yield a closer estimate of the optimal fit between the two selected VDS microscopy images.

4.5.1 Rotation

The rotation is estimated as the next step of the rigid registration. To estimate the rotation the data is converted to a polar representation. This is done to get a measure of the rotation with the 2D cross-correlation method using FFT. The transformation of the data to a polar representation is described in the following section.

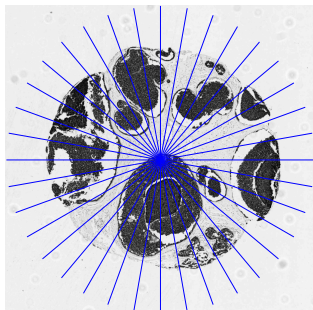
4.5.2 Polar representation

To estimate the angle θ in the rotation parameter \mathbf{R} , a polar representation of the data is generated. The generation is executed in MATLAB by the use of the command `pol2cart`. The images in Cartesian coordinate systems are transformed as if they were Polar-coordinates. The transformation is given as the following.

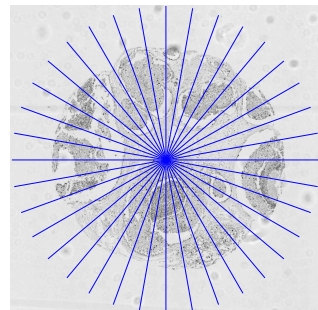
$$x = \rho \cdot \cos(\theta_p) \quad (4.5)$$

$$y = \rho \cdot \sin(\theta_p) \quad (4.6)$$

Here x and y are Cartesian coordinates, ρ is the sampling along the wheel spoke and θ_p is the angle of the wheel spoke in the polar coordinate system. This yields a Polar representation of the images displayed in figure 4.5, the blue lines indicates the sampling along the wheel spokes at an angle θ_p .



(a) TMA core stained with PCK



(b) TMA core stained with Ki-67

Figure 4.5: Illustration of the generated polar representation. The blue lines indicates the samples along the wheel spokes. The wheel spokes are only displayed at every ten degrees to illustrate the concept. In the implemented version the wheel spoke frequency of 8 wheel spokes per degree.

The blue lines in figure 4.5 illustrates the concept of the sampling along wheel spokes to generate the polar representation. In the illustration the wheel spoke frequency is one wheel spoke every 10th degree. For the extracted polar representation in the algorithm, the wheel spokes frequency is 8 wheel spokes

per degree. It is noticed that the area near the origin of the wheel spokes gets overrepresented.

After the polar data points are extracted the result from the polar representation of the two images

The results of the two images converted to polar representations can be seen in figure 4.6 and 4.7. The x-axis represents the angle (θ) of the wheel spokes and the y-axis denotes the sampling along the wheel spokes.

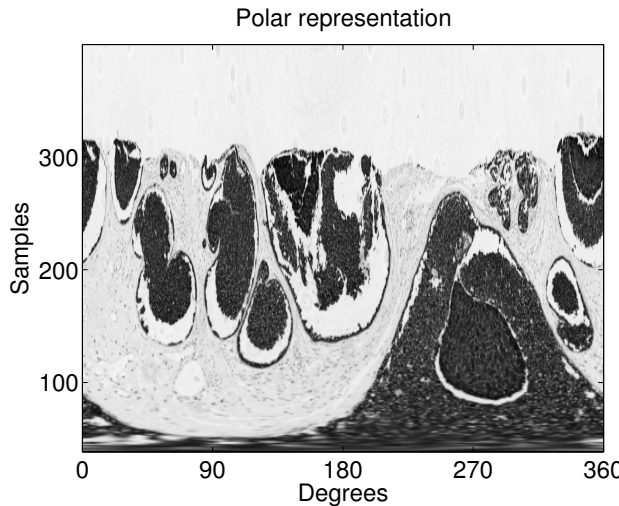


Figure 4.6: Polar representation of the virtual microscopy image displayed in figure 4.3(a) stained with PCK. The x-axis denotes the angle (θ) of the wheel spokes. y-axis denotes the sampling along the wheel spokes.

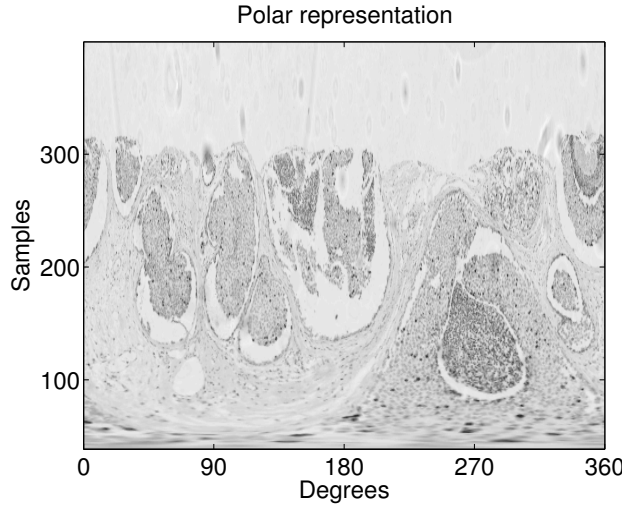


Figure 4.7: Polar representation of the virtual microscopy image displayed in figure 4.3(b) stained with KI-67. The x-axis denotes the angle (θ) of the wheel spokes. y-axis denotes the sampling along the wheel spokes.

The two polar representations are now used as input in the translation estimation described in section 4.4.1 and 4.5. It is assumed that a rotation can be estimated as the relation in translation t_r between the two polar representations I_{P1} and I_{P2} in the x direction. The polar representation is initiated at 0 degrees in the world coordinates independent of the placement and rotation of the core. This makes it possible to use the estimated translation parameter t_r in the x direction to estimate the angle θ in the rotation parameter \mathbf{R} .

The same procedure as described in section 4.5 is executed. The two polar representations are used as input in the translation estimation. First the FFT is used to calculate the 2D Fourier Transformation, then they are multiplied where one is complex conjugated. This is followed by the 2 D Inverse Fourier Transform where the maximum of the result reveals the possible translation in the x direction, hence the rotation of the core relative to the other. The 2D IFFT of the two images is displayed in figure 4.8 where the green sphere indicates the maximum. The IFFT result is not visualized as the fftshifted, since it is easier to locate the direction of the translation t in the non fftshifted.

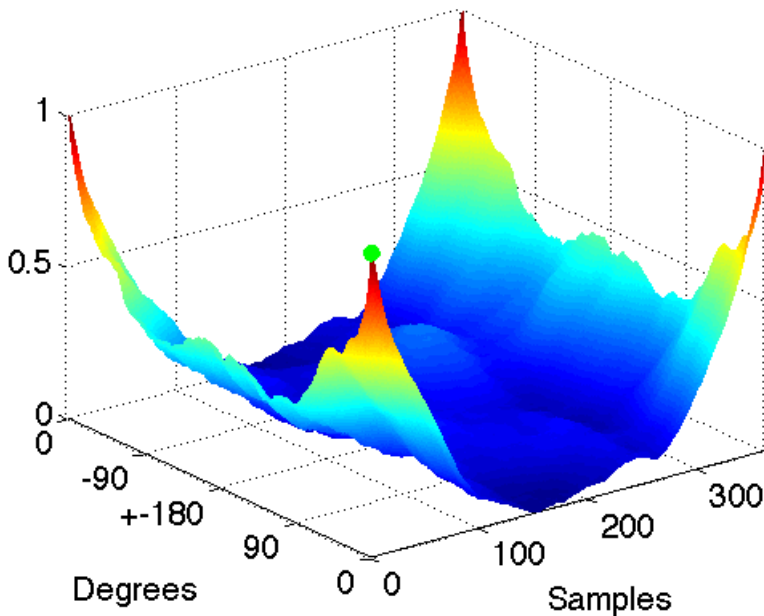


Figure 4.8: 2D Inverse Fourier Transform of the polar representation of the serial slice cores in figure 4.3. The green sphere indicates the maximum and depicts the relation in the rotation angle θ between the two images. For these two images the relation in rotation is found to be 0.25 degrees.

The estimated rotation is for this particular case found to be 0.25 degrees and can be applied as described in section 2.4 to come closer to estimating the optimal fit.

4.6 Iterative rigid registration process

The optimal translation and rotation parameters are estimated through an iterative process illustrated by the flow diagram in figure 4.9. The first step in the iterative registration process is an initial translation estimation which is applied to generate a good initial guess for estimating the angle θ in the rotation parameter. This is done because the rotation parameter estimation is more affected by a poor initial guess. The application of the deformation in

the first iteration is written in equation 4.7

$$Y = R(x + t) \quad (4.7)$$

The translation parameter t is applied to the original image I_2 yielding a new transformed image I'_2 . The new transformed image is then used as input in the estimation of the rotation. The rotation parameter is then estimated with the polar representation. If the angle θ in the rotation is estimated to a value different from zero degrees, the rotation is applied to I'_2 and the process is repeated. This is continued until the angle θ in rotation parameter is estimated to zero, then the rigid registration process has found the best estimation of the translation parameter t and the angle θ in the rotation parameter \mathbf{R} .

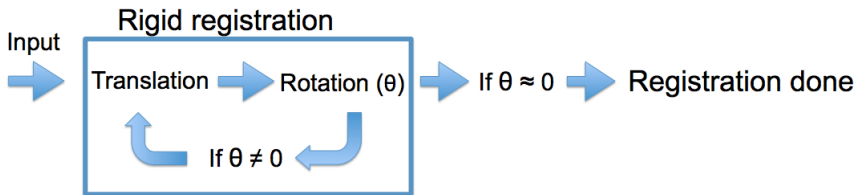


Figure 4.9: Flow diagram of the iterative rigid registration process. The process continues until a value of zero degrees is estimated for the the angle θ in the rotation parameter.

The iterative rigid registration process could cause an interpolation error if the registration parameters are updated over several iterations. The image with interpolations error could be seen as a blurred or smoothed image due to the large number of mean estimations of the transformed pixel values. Different interpolation methods are available with different advantages and disadvantages. A bicubic interpolation is used in this project.

To minimize this interpolation error the deformation field is updated after each iteration. This yields only one conducted interpolation after each calculation of the parameters and one conducted interpolation from the original image to the transformed image. The iteratively updated deformation field Y' is expressed in equation 4.8.

$$Y' = \mathbf{R}_{i+n}(\dots\mathbf{R}_{i+2}(\mathbf{R}_{i+1}(\mathbf{R}_i(x_i + t_i) + t_{i+1}) + t_{i+2})\dots t_{i+n}) \quad (4.8)$$

where Y' is the deformation field after all iterations $i + n$, \mathbf{R} is the rotation parameter and t is the translation parameter.

4.7 Weighting and limitation

The basic algorithm was tested on the full dataset to study if it could register all the tissue samples in the dataset. This was conducted as a trial and error test without any statistical involvement at this point. The study showed that the basic algorithm was unable to align all of the cores in the dataset. When assessing the cores that failed the alignment it was revealed that in some cases an unrealistic maximum was detected with the 2D cross-correlation. This resulted in an unknown error in the estimate of the registration parameters and because this transformation is used as the input in the next estimation of the registration parameters a series of wrong estimates were created. An example of this phenomenon is shown in figure 4.11 and 4.12, with the cores presented in 4.10 as input, I_1 and I_2 .

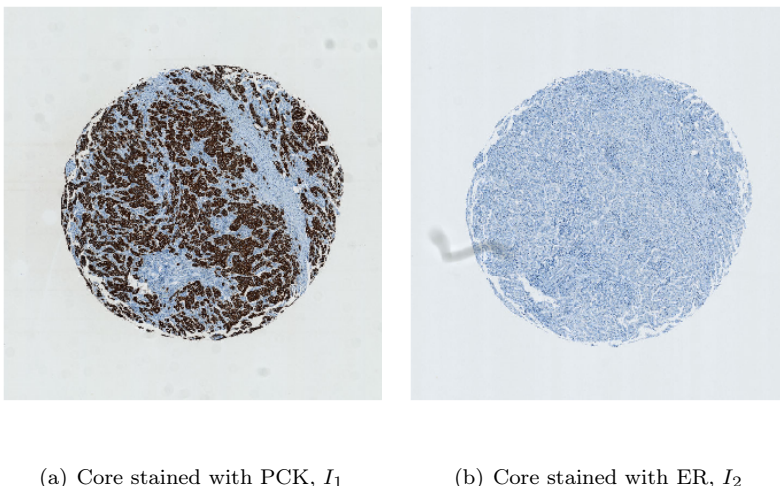


Figure 4.10: Serial sliced cores stained differently with PCK and ER. The cores are used to illustrate the effect of applying a weighting of the 2D IFFT cross-correlation.

The first estimation of the translation parameter t showed a translation of 6 pixels in the x-direction and 2 pixels in the y-direction. Then the first estimation of the angle θ in the rotational parameter \mathbf{R} show a rotation of -165.625 degrees as the best fit. This correlation estimate is displayed in figure 4.11. As described in section 4.2 it is unlikely that a cores have been rotated around 180 degrees, if so it would have been detected in the data extraction process if the guidelines were followed.

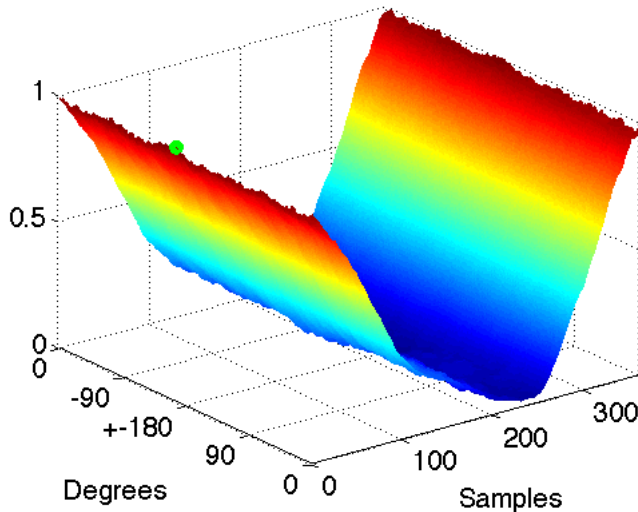


Figure 4.11: 2D IFFT cross-correlation of the polar representation of the differently stained serial sliced core in 4.10. The green sphere marks the maximum detected for estimating the rotational parameter \mathbf{R} . The angle θ in the rotational parameter is estimated to -165.625 degrees which contradicts the assumptions made from the guidelines described in section 4.2.

The estimation of the rotational parameter \mathbf{R} , in figure 4.11, now yields the input data for the next iteration for estimating the translation parameter t . This input results in a large estimated translation visualized in figure 4.12. Here the estimated translation is -280 pixels in the x-direction and -218 pixels in the y-direction.

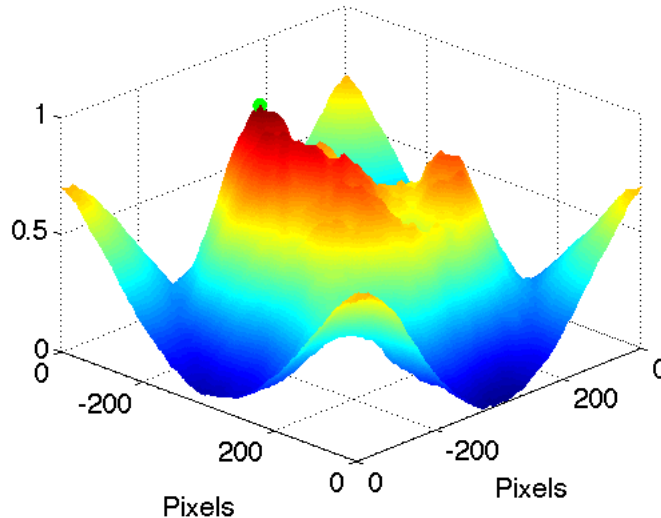


Figure 4.12: 2D IFFT cross-correlation of the transformed image I'_2 from figure 4.8. The green sphere marks the maximum detected for estimating the translation parameter t . The translation parameter is estimated to -280 pixels in the x-direction and -218 pixels in the y-direction. This estimation contradicts the assumptions made from the guidelines described in section 4.2.

As stated in section 4.2 when extracting the cores a grid is placed on top of the cores before de-arrying the cores. This is done semi automatically with a TMA core detection algorithm in Visiopharm's software and a manual correction of the cores that are poorly detected. It is assumed that the extracted cores are nearly centred when being de-arrayed indicating that a translation of -280 pixels in a 700x700 pixel images is unlikely. It is also assumed that a rotation of 90-180 degrees is detected in the extraction process.

A weighting can be implemented on the inverse Fourier Transform of the cross-correlation. A weighting that favours small translations over of large translations is preferable. An inverse 2D Hamming window is chosen as the weighting and is implemented in the x and y directions. The weighting is visualized in figure 4.13.

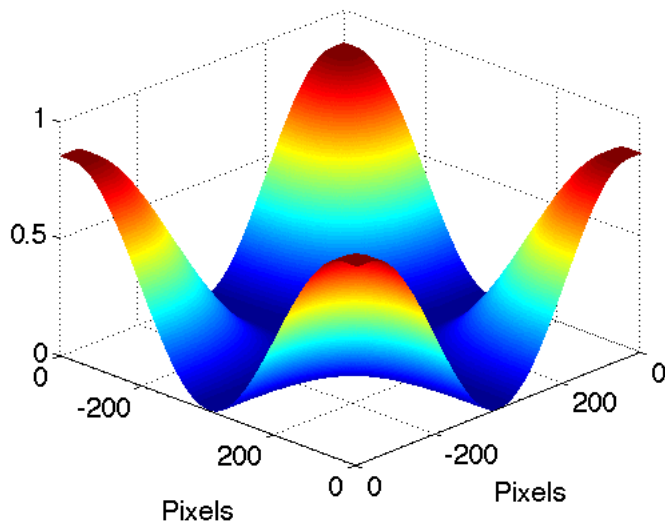


Figure 4.13: Illustration of the weighting translation estimation. 2D Hamming weighted window generated after ± 30 pixel step in the x and y directions.

The 2D Hamming weighting window presented in figure 4.13 is implemented before and after a ± 30 pixel step in the x and y directions. This means that if the translation is larger than 30 pixel the weighting is applied. This implementation favours small translations and applies a weight if the translation is larger than ± 30 pixel in the x and y directions.

The weighting is expanded to also discard values lower than -75 pixels and higher than 75 pixels in the x and y directions. This limited 2D Hamming weighting is visualized in figure 4.14

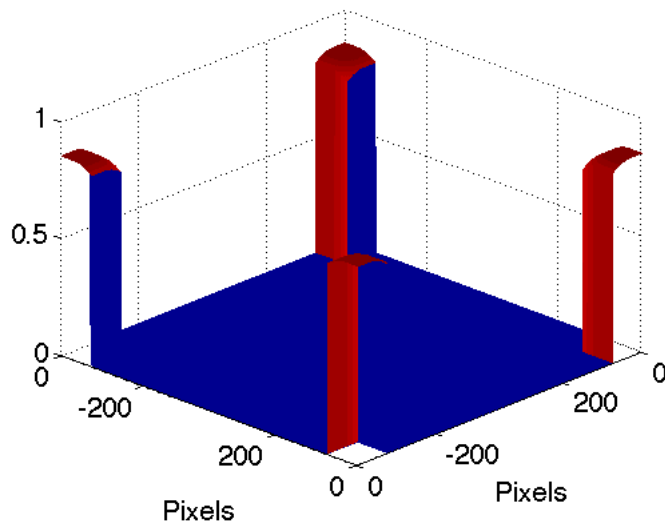


Figure 4.14: The limited weighting of the translation estimation. 2D Hamming weighted window generated after ± 30 pixels and limited to ± 75 pixels in the x an y directions.

This limitation forces the estimation of the translation parameter to be within ± 75 pixels and the weighting favours translations between ± 30 pixels. The values for the limitation and the weighting are based on empirical measures and are tested on the whole dataset. The criteria was that the registration reached an estimated translation without error. The limited weighting was applied to the 2D IFFT correlation displayed in figure 4.15. Now the same translation showed a more likely estimation of the translation.

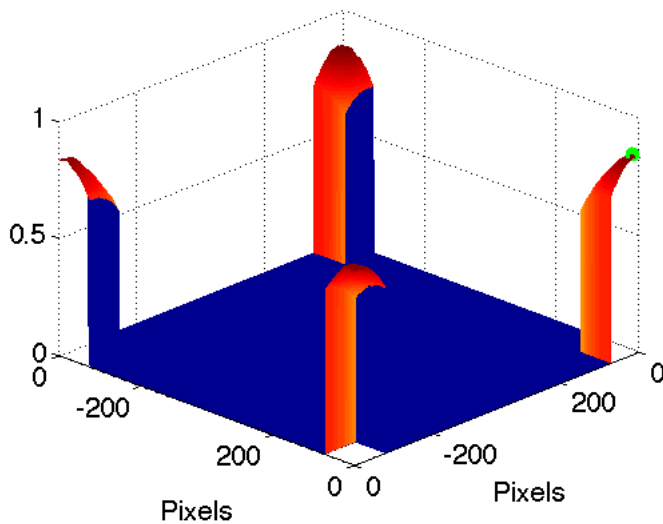


Figure 4.15: The limited weighting displayed in figure 4.14 applied to the 2D IFFT cross-correlation of the transformed image I'_2 from figure 4.8. The green sphere marks the new maximum detected for estimating the translation parameter t . The first translation is estimated as the same to 4 pixels in the x-direction and 12 pixels in the y-direction.

A limited weighting is also applied to the 2D IFFT of the polar 2D cross-correlation. This is done to favour small degree estimations. The weighting is displayed in figure 4.16.

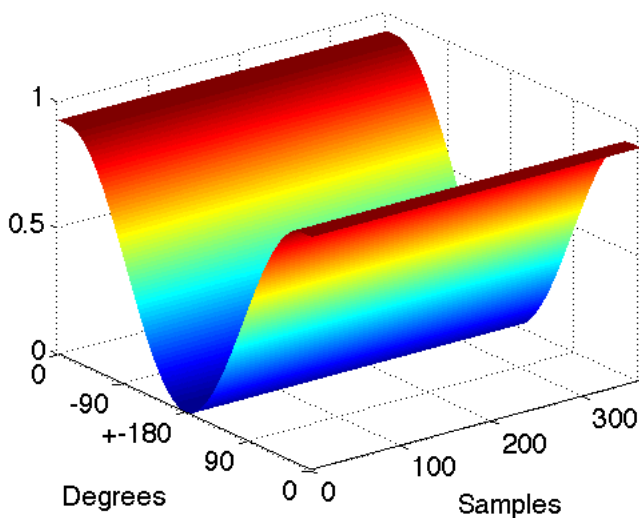


Figure 4.16: The weighting of the 2D IFFT cross-correlation of the polar representation for estimating the rotational parameter. 2D Hamming weighted window generated after a step of 8 degrees in the x direction.

In figure 4.16 a Hamming weighted window is generated after a step of 8 degrees in the x direction repeated in the y direction. This creates a 2D weighting that favours small degrees, that is estimated from the x-coordinate of the maximum values. A limitation is also applied to discard all rotations lower than -15 and higher than 15 degrees displayed in figure 4.17.

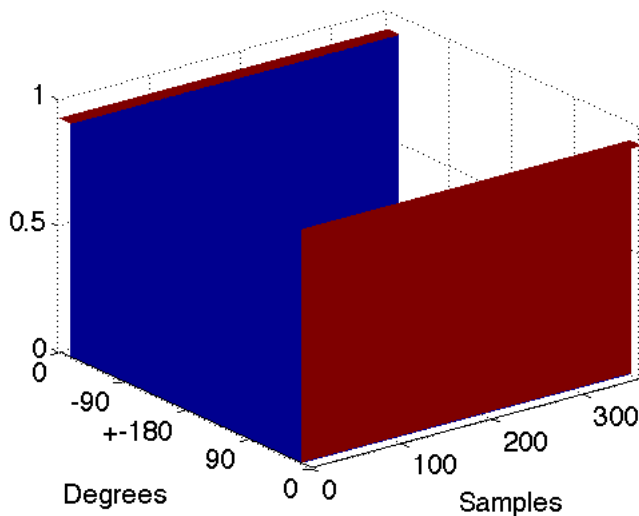


Figure 4.17: The limited weighting of the 2D IFFT cross-correlation of the polar representation for estimating the rotational parameter. 2D Hamming weighted window generated after a step of 8 degrees and a limit of 15 degrees in the x direction and duplicate in the y direction

The 2D limited hamming weighting is applied in the estimation of the angle of rotation in figure 4.18. The estimation of θ is now -0.50 degrees instead of the -165.625 degrees estimated in 4.11. This indicates that a more likely registration has been estimated.

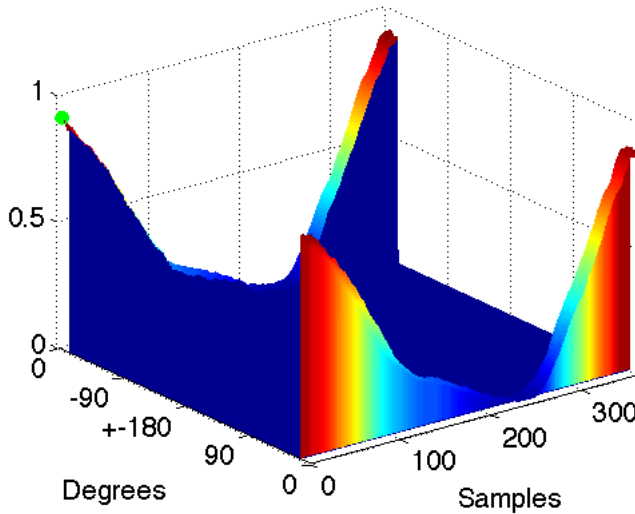


Figure 4.18: The limited weighting displayed in figure 4.17 applied to the 2D IFFT cross-correlation of the transformed image I'_2 from figure 4.8. The green sphere marks the new maximum detected for estimating the rotational parameter \mathbf{R} . The new estimate of the rotational parameter is equal to -0.50 degrees.

The weighted limitation of the 2D cross-correlation in the estimation of the translation and rotation parameters now favours small steps. This prevents the correlation from estimating a wrong parameter value that contradicts the assumptions made from the guidelines described in section 4.2. The registration result after applying the weighting and the limitation is displayed in figure 4.19.

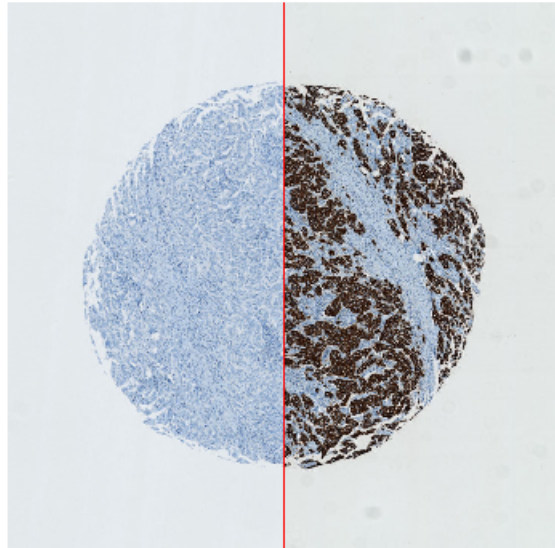


Figure 4.19: Registration result of the cores displayed in figure 4.10, after applying the weighting and the limitation.

4.8 Zeropadding

When conducting the rigid transformation with the FFT based method the images used as input are required to have the same size. This is essential when multiplying the image matrices in the Fourier domain. When applying the estimated translation or rotation parameter the images need to be reduced in size or be zero padded to uphold this requirement. When changing the size of the images it becomes difficult to compare them e.g. when calculating Mutual Information which is dependent on the amount of pixels in the image. The method of adding zeroes to the image could affect the registration and yield incorrect results.

To overcome the reduction or zero padding of image another larger image is extracted for all cores to use as an original image. These images makes it possible to translate and rotate the field of view without having to reduce or include zero padding in the images. The process of translating and rotating the field of view is illustrated in figure 4.20.

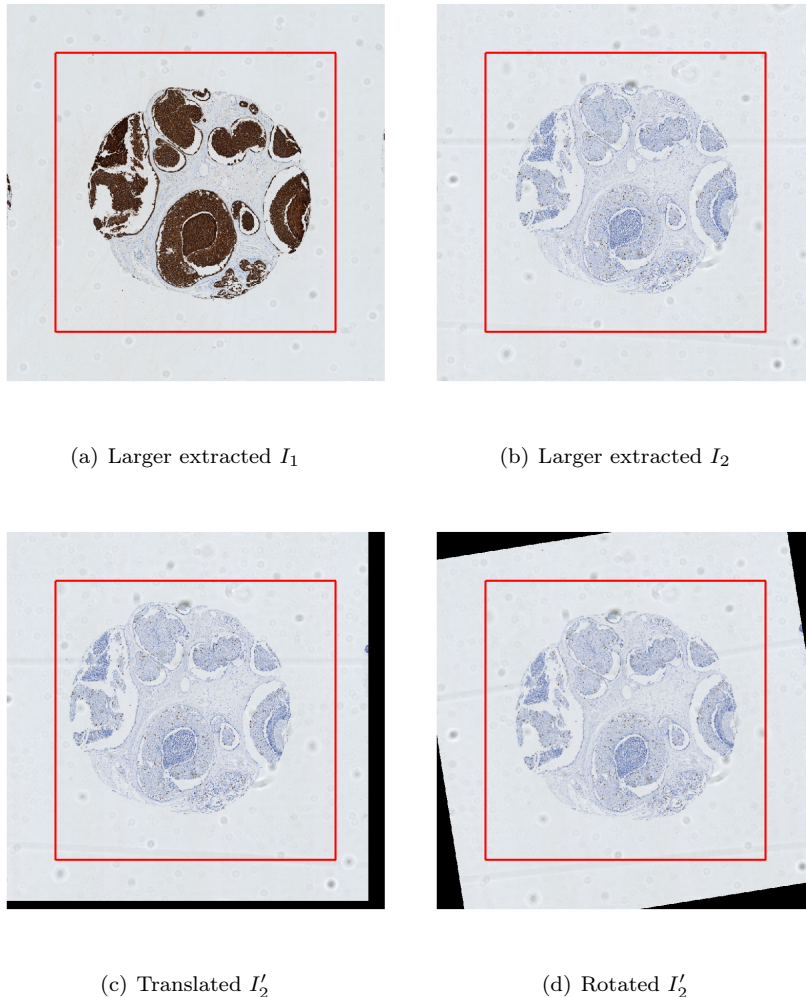


Figure 4.20: Illustration of the Field of view (FoV) in the larger extracted image. The red square visualizes the FoV used to display the tissue sample. everything outside of the red square is not visualized. a) Larger reference image I_1 extracted with defined FoV. b) Larger transformation image I_2 extracted with defined FoV. c) The FoV is steady and the larger extracted image I_2' is translated, this yields no cropping or zero padding within the FoV. d) The larger extracted I_2' is applied a rotation and the FoV is held steady this yields no zero padding of the within the FoV. The rigid transformation parameters applied in this illustration is not estimated and is only applied to illustrate the process.

The illustration in figure 4.20 displays the rotation and translation of the larger extracted image, maintaining the Field of View within it. The amount of rotation and translation is of course limited to the size of the larger extracted image. In the illustration in figure 4.20 the limitation in rotation before having to zero pad is 30 degrees. A larger image could be extracted to be able to rotate the extracted image 45 degrees but since none of the cores in the dataset is expected to have a rotation $\theta > 20$ degrees, this size is sufficient. The translation is limited to 120 pixel before zero padding or cropping of the transformed image is needed. As described in a previous section the TMA cores are automatically centered followed by a manual inspection and this prevents the translation parameter t to exceed the 120 pixels.

4.9 Phantom

When performing image registration on real life images such as medical images, the difficult part is that the ground truth is usually unknown. This yields the difficult task of validating the results obtained by an image registration algorithm. In this project it is assumed that the two serial sliced sections of mamma tissue are considered to have share major tissue characteristics. This makes it difficult to determine the exact match of the tissue samples, since they are not completely identical and stained differently.

In a search of a method to validate the FB algorithm a simple TMA core phantom is generated to simulate two identical tissue samples related by a rigid registration. The phantom is generated as a grey scale image where different intensities are applied in multiple regions to simulate different features from the staining. The phantom is inspired by the Shepp Logan phantom used in CT back projection simulation.

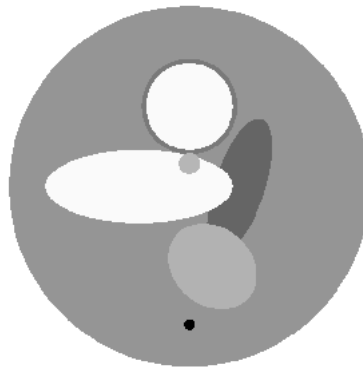


Figure 4.21: Phantom of a TMA core generated to quantify the performance of the FB algorithm. The TMA phantom core is created to have features equivalent to a TMA mamma tissue biopsy and is given in pixel values from 0 to 1.

To study the FB algorithm, different known rigid transformations are applied to the phantom. The transformations consist of different translations and rotations. The results of the registrations with the FB registration method are evaluated using Sum of Squared Difference, the results are displayed in section 5.1.

4.10 Pre-processing tests

When conducting the image registration, pre-processing should be considered to emphasize possible information hidden in the images. In the preliminary study for developing the rigid registration method for VDS, different pre-processes were tested to see if they yielded a better result.

The pre-processing were applied in an attempt to equalize the differences between the staining results. The different stains emphasize different features in form of color and intensities. A Gabor filter is applied to detect the structures and even out the differences between the different stains.

The variation from the different staining procedures also suggest to study the colorbands. Chromaticity isolates the different colorbands and reduces the intensity dependency. All combinations of calculated chromaticities are tested with the different staining procedures and colorbands to study if a certain combination yielded better results.

None of pre-processes tested showed overall improvements. The pre-processing did not get implemented in the final registration model. This section describes the pre-processes that has been tested to document them for future knowledge.

4.10.1 Gabor filter

The rigid registration relies on structures and intensities within the microscopic images. This suggests applying some sort of filter before performing the registration.

The Gabor filter is a linear filter used for edge detection. The Gabor-filter is known to be preferable for texture representation and discrimination. The following section displays the Gabor-filter and the result after application on a set of TMA core images.

The Gabor-filter is displayed in figure 4.23. The only parameter changed in the test is the wavelength of the filter λ . The filter is displayed for $\lambda = 2$ in figure 4.22 and for $\lambda = 8$ in figure 4.23. The filter is applied in 8 directions and the results are summed to generate a final normalized filtered image.

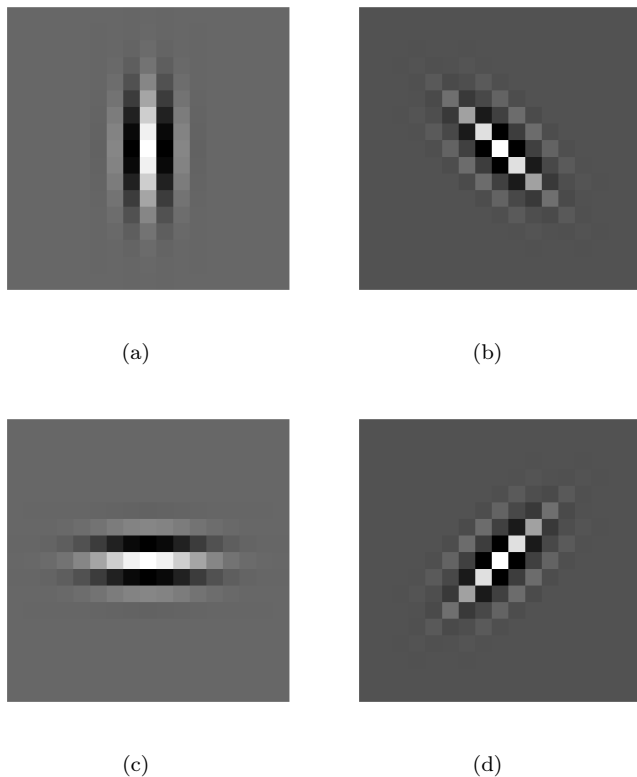


Figure 4.22: Gabor-filter displayed in four orientations, all filters are applied in both directions perpendicular on the filter to the image. The parameters used to generate the Gabor-filter are $\lambda = 2$, $\gamma = 0.5$ and a bandwidth = 1.

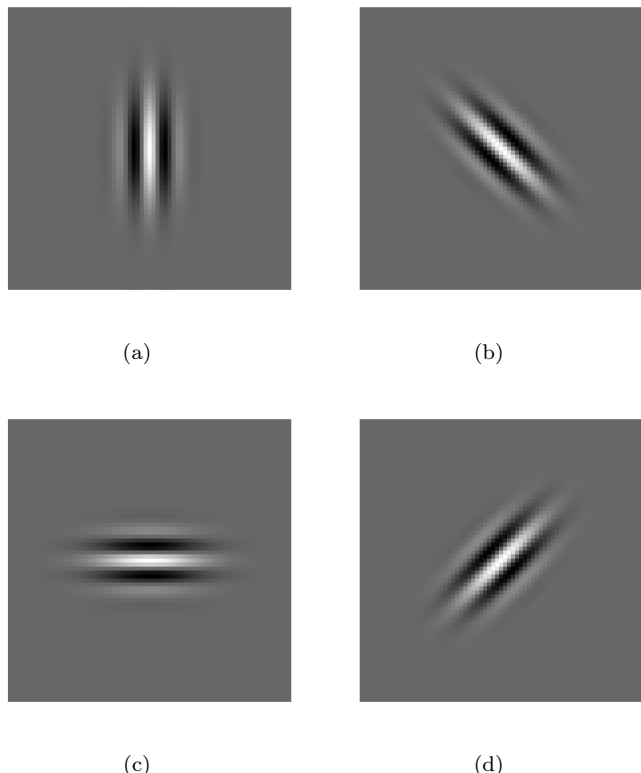
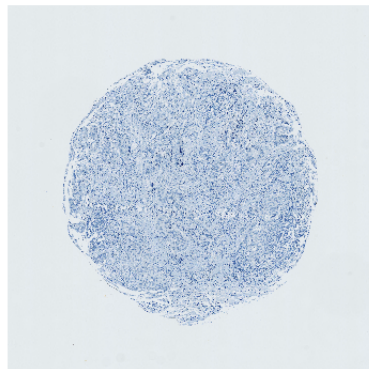
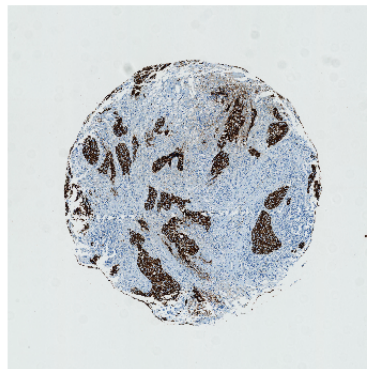


Figure 4.23: Gabor-filter displayed in four orientations, all filters are applied in both directions perpendicular on the filter to the image. The parameters used to generate the Gabor-filter are $\lambda = 8$, $\gamma = 0.5$ and a bandwidth = 1.

The Gabor-filter is applied to the grey scale conversion of the serial sliced TMA cores in figure 4.24. The images in figure 4.26, 4.25 and 4.27 displays the filter applied with different values of λ .

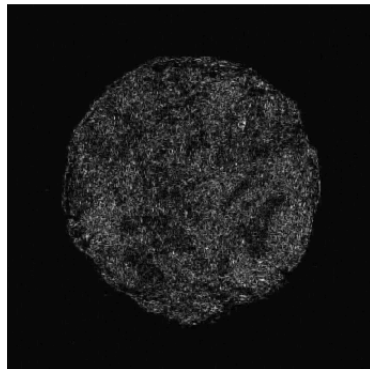


(a) TMA core stained with ER

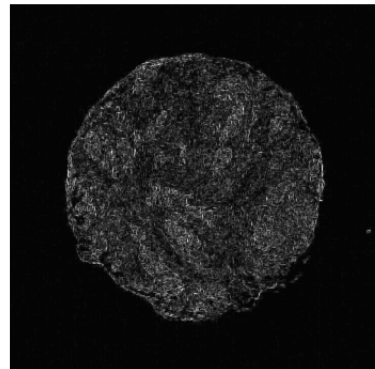


(b) TMA core stained with PCK

Figure 4.24: Example TMA cores used to illustrate the Gabor filter.

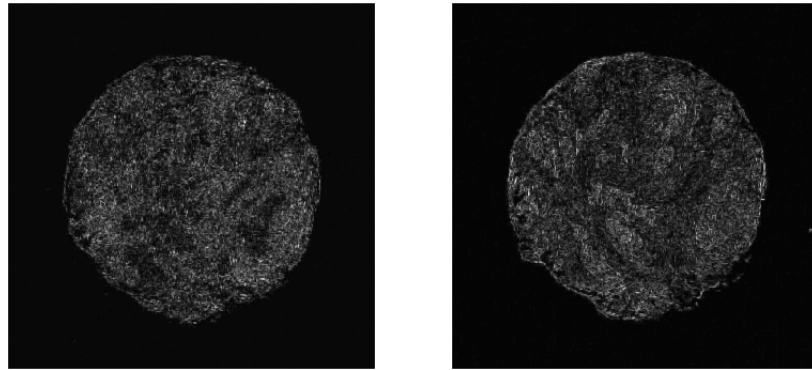


(a) TMA core stained with ER



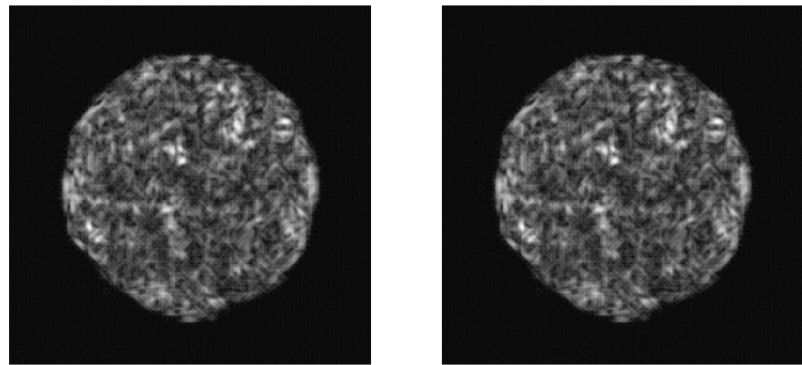
(b) TMA core stained with PCK

Figure 4.25: Gabor-filtered grey-scale images with $\lambda = 2$.



(a) TMA core stained with ER

(b) TMA core stained with PCK

Figure 4.26: Gabor-filtered grey-scale images with $\lambda = 3$.

(a) TMA core stained with ER

(b) TMA core stained with PCK

Figure 4.27: Gabor-filtered grey-scale images with $\lambda = 8$.

It can be seen from the images in figure 4.26, 4.25 and 4.27 that with larger wavelengths the edges get more blurry in the filtered image. Larger wave lengths turn out to have a negative effect on the FB rigid registration. Values of $\lambda = 2$, $\lambda = 3$ and $\lambda = 4$ were chosen to test the effect of the Gabor-filter.

In the test of the Gabor filter increased the number of iterations to a mean of approximately 10 iterations. This is not preferable since it indicates difficulty in estimating the optimal registration parameters. Numerous times the registration of the cores stopped because the parameters for the translation t and rotation \mathbf{R} exceeded the image boundaries indicated by an error. This indicates that the Gabor-filter with the chosen λ values did not improve the registration and was therefore not implemented in the final registration algorithm.

4.10.2 Chromaticity

The Chromaticity is calculated for each of the RGB - channels and tested on all combinations of staining procedures. The study would show if there was a combination that equalized the differences caused by the different IHC processes. The chromaticity is calculated for the three color channels as given in equation equation 4.9, 4.10 and 4.11. The chromaticity is applied to all the pixels in the image.

$$R = \frac{R}{R + G + B} \quad (4.9)$$

$$G = \frac{G}{R + G + B} \quad (4.10)$$

$$B = \frac{B}{R + G + B} \quad (4.11)$$

An example of the chromaticities calculated for a core stain with PCK and Ki-67 is presented in figure 4.28, 4.29, 4.30 and 4.31. The different chromaticity calculations are used as the input in the FB registration method and all combinations are tested.

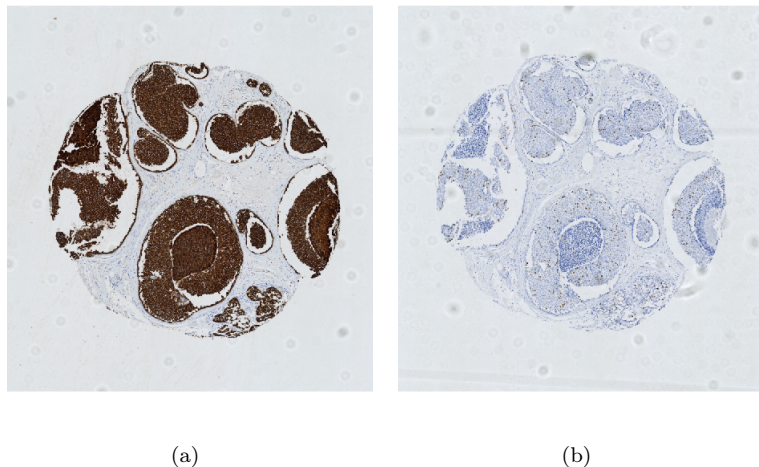


Figure 4.28: Microscopy images of a serial sliced TMA core. a) Tissue stained with PCK which is a marker for epithelial cells. b) Tissue stained with KI-67 which is a cell nucleus marker that can determine the amount of cellular division.

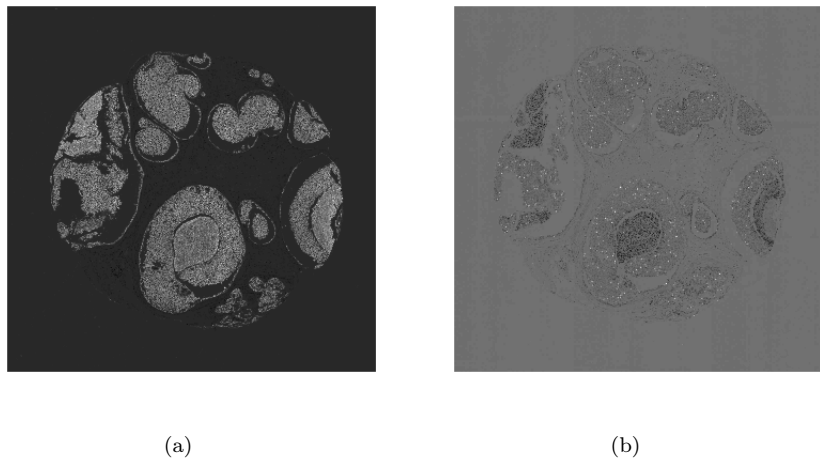
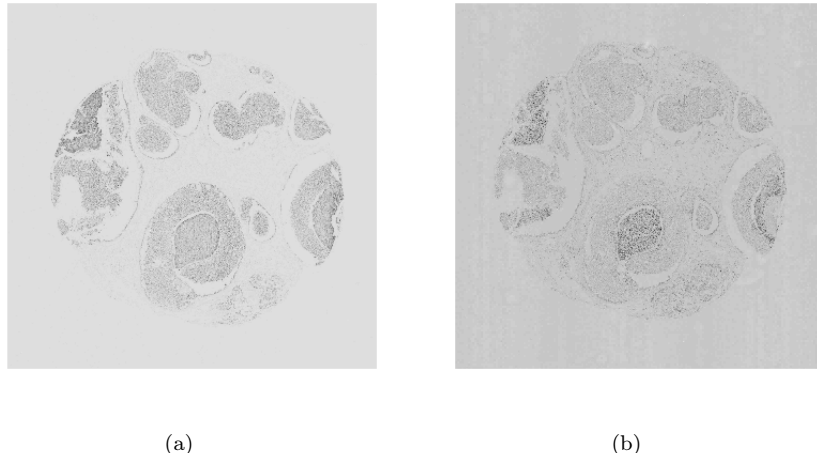


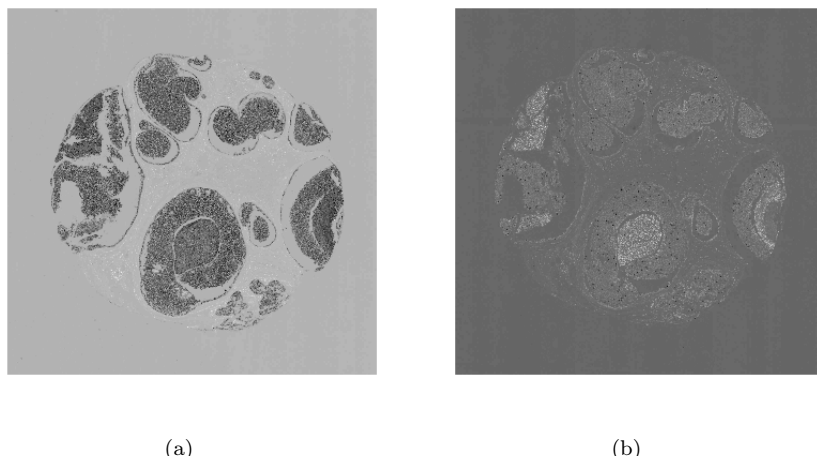
Figure 4.29: Chromaticity of the red-channel, calculated according to equation 4.9. a) Stained with PCK. b) Stained with KI-67.



(a)

(b)

Figure 4.30: Chromaticity of the green-channel, calculated according to equation 4.10. a) Stained with PCK. b) Stained with KI-67.



(a)

(b)

Figure 4.31: Chromaticity of the blue-channel, calculated according to equation 4.11. a) Stained with PCK. b) Stained with KI-67.

None of the chromaticity combinations yielded a consistent improved registration result across the different stains. The different chromaticity calculations did not even out the difference induced by the staining. The

chromaticity was not used in the final registration algorithm.

4.11 Manual registration

To establish a rigid registration result to compare with the FB rigid registration, a manually Point based (PB) rigid registration is conducted. This is done to quantify if the FB registration is as good as a manual PB registration. The generated statistical analysis for comparing the two forms of rigid registrations is described in section 5.4.

The PB registration is conducted by a group of 4 test subjects, 2 Medicine and technology students and 2 Medical Doctor student all in their last year of studying. The PB registrations are performed on a random selected dataset of 50 cores described in section 5.2. All batches are represented and the staining processes are randomized. Four annotation point are used in the rigid registration and the GUI created for placing the annotations is displayed in figure 4.32.

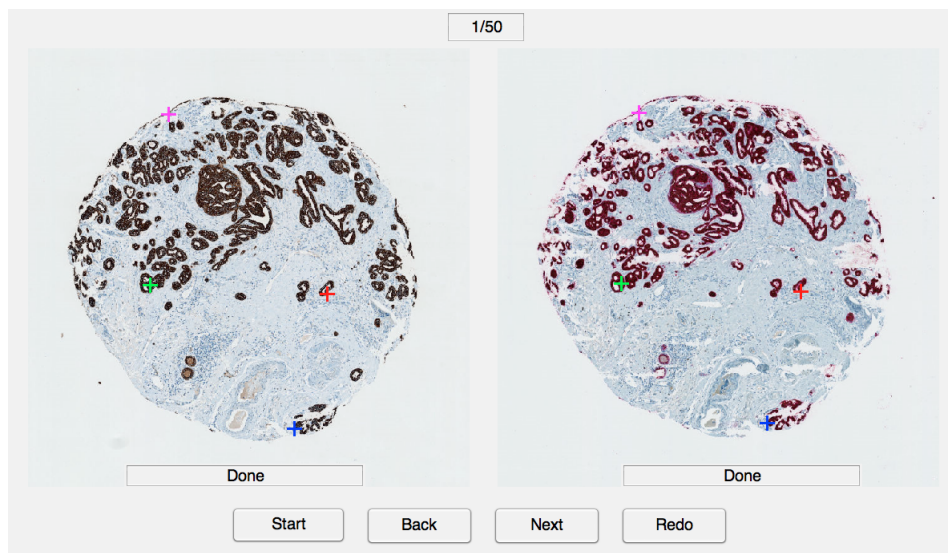


Figure 4.32: Created GUI for Point Based rigid registration. The test subjects are bound to place four annotation point at individually assessed similarities in the images. The dataset consists of image pairs that are serial sliced TMA cores stained differently. The annotation points are paired in colour to annotate chosen similarities. The first annotation point is red. The second annotation point is blue. The third annotation point is magenta. The fourth annotation point is green.

The GUI is created in MATLAB and is generated to be as simple as possible to make the test subjects focus on the registration instead of complicated GUI steps. After pressing start, the first core for placing annotation points appears. After placing the four annotation points at individually assessed similarities in the images, the test subjects click next and a new core appears. The test subjects also have the choice of redoing the annotation by clicking redo. The test subjects does not see the transformed result of their annotation points to simplify the process. The test subjects were instructed on how to use the GUI and told to avoid placing the annotation points in a small pile, to minimize the error induced by the uncertainty in placing the annotation points. The PB registration method is based on Procrustes theory, described in the following section.

4.11.1 Point based rigid registration

The translation in the x and y directions is calculated as the difference between the centroid of the two sets of annotation points. It can be written as the following [5].

$$\bar{x} = \frac{\sum_k^N w_k^2 x_k}{\sum_k^N w_k^2} \quad (4.12)$$

$$\bar{y} = \frac{\sum_k^N w_k^2 y_k}{\sum_k^N w_k^2} \quad (4.13)$$

Where x is the first set of the annotation points and y is the second set of annotation points. k denotes the annotation point. The weighting w is set to 1. The translation can now be found by subtracting the two centroids. To calculate the rotation the displacement from each point to the centroid is calculated as the following [5].

$$\tilde{x} = x_k - \bar{x} \quad (4.14)$$

$$\tilde{y} = y_k - \bar{y} \quad (4.15)$$

The covariance matrix is then computed

$$H = \sum_k^N w_k^2 \tilde{x}_k \tilde{y}_k^t \quad (4.16)$$

Singular value decomposition of H is then performed.

$$H = U \Lambda V^t \quad (4.17)$$

where $U^t U = V^t V = 1$, $\Lambda = \text{diag}(\lambda_1, \lambda_2, \lambda_3)$, and $\lambda_1 \geq \lambda_2 \geq \lambda_3 \geq 0$

the rotation θ is then calculated as

$$\theta = V \text{diag}(1, 1, \det(VU)) U^t \quad (4.18)$$

The results from the PB registration of the random selected 50 cores are then analysed and compared with the results from the FB registrations of the same 50 cores. The results are presented in chapter 5 and discussed in chapter 6.

4.12 Statistical analysis setup

Prior to the statistical analysis we assumed that the VDS procedure is followed before performing the registration and the two serial slice tissue samples share major tissue characteristics. Furthermore when applying the different staining procedures the tissue can change information within the major shared characteristics. This makes it almost impossible to try to find the ground truth for comparison.

In order to get an impression on the quality of the fit from the FB registration method, a group of four test subjects conducted PB registration on a randomly selected subset of 50 cores described further in section 5.2.

To compare the manually conducted PB rigid registration and the FB rigid registration, the deformation fields (Y) that are calculated to transform the images are compared. For the PB registration the deformation field (Y_{PB}) is calculated as equation 2.1 and shown in 4.19. Here only one rotational parameter \mathbf{R} and one translation parameter t is estimated.

$$Y_{PB} = \begin{pmatrix} \cos(\theta) & -\sin(\theta) \\ \sin(\theta) & \cos(\theta) \end{pmatrix} \begin{pmatrix} x \\ y \end{pmatrix} + \begin{pmatrix} t_x \\ t_y \end{pmatrix} \quad (4.19)$$

The x and y are the original coordinates, t_x and t_y are the translation parameters and θ is the angle of the rotation parameter \mathbf{R} . The deformation field for the FB registration (Y_{FB}) is calculated in equation 4.20. A difference from the PB registration is that the translation is applied before the rotation and the deformation field is calculated as an iterative process as given previously in equation 4.8.

$$Y_{FB} = \begin{pmatrix} \cos(\theta) & -\sin(\theta) \\ \sin(\theta) & \cos(\theta) \end{pmatrix} \left(\begin{pmatrix} x \\ y \end{pmatrix} + \begin{pmatrix} t_x \\ t_y \end{pmatrix} \right) \quad (4.20)$$

The x and y are the original coordinates, t_x and t_y are the translation parameters and θ is the angle of the rotation parameter \mathbf{R} . The experimental setup for this analysis is listed in table 4.1.

Table 4.1: Experimental setup.

Design of experiment	
Method	Number of deformation fields
Visiopharm's method (VIS)	0
Fourier based method (FB)	1
Point based method (PB)	
Test subject 1	1
Test subject 2	1
Test subject 3	1
Test subject 4	1

The result obtained by Visiopharm's method did not yield any deformation field as the registration parameters were unable to be extracted at this point. The deformation field estimated by the test subject and the deformation field estimated by the FB method may be compared. Since there are no ground truth deformation field available, we compare the FB deformation field with the deformation field from test subjects to study if the deformation fields are significantly different from each other. The deformation field is given as

$$Y = \sqrt{Y_x^2 + Y_y^2} \quad (4.21)$$

Here Y is the length of the deformation in the x and y direction. Y_x is the deformation in the x direction and Y_y is the deformation in the y direction. We now define the distance between two deformation fields as the norm of two deformation fields written as the following.

$$\|Y_1 - Y_2\| = \sum_i \|Y_1(i) - Y_2(i)\| \quad (4.22)$$

Here the Y_1 is the first deformation field and Y_2 is the second deformation field. The difference in deformation are calculated as a distance for each pixel i . The difference in the FB deformation field and the PB deformation field is to be compared. An approximative solution could be the following adapted statistical analysis denoted as the ad hoc setup.

$$F_j = \frac{\|Y_{FB_j} - \bar{Y}_{PB_j}\|^2}{\left(\sum_{n=1}^4 \|Y_{PB_{nj}} - \bar{Y}_{PB_j}\|^2\right)/3} \quad (4.23)$$

Here Y_{FB_j} is the deformation field from the Fourier based registration of core j , $Y_{PB_{nj}}$ is the deformation field from the PB registration from test subject n of core j , and \bar{Y}_{PB_j} is the mean deformation field of the PB registration from the four test subjects of core j . If we in the numerator assume that \bar{Y}_{PB_j} is the "true" deformation field this quantity resembles an F-test with (1,3) degrees of freedom.

To test Visiopharm's registration of the extracted dataset other measures have to be considered since the deformation field is missing. As presented in section 2.5 Mutual Information could be an estimate of the quality of the alignment. If we assume that MI is a good measure of the alignment between the cores, it could be used in the following ad hoc setup.

$$t_j = \frac{MI_{FB_j} - \bar{MI}_{VIS_j}}{\left(\sqrt{\sum_{n=1}^4 (MI_{PB_{nj}} - \bar{MI}_{PB_j})^2} \right) / 3} \quad (4.24)$$

here j is the core number, MI_{FB_j} is the Mutual Information of the FFB registration, MI_{VIS_j} is the Mutual Information of Visiopharm's alignment. $MI_{PB_{nj}}$ is the Mutual Information of the PB registration from test subject n and \bar{MI}_{PB_j} is the mean Mutual Information of the PB registration from the four test subjects. If we assume that the MI results are normally distributed this could be tested against a t -distribution with 3 degrees of freedom. The results from these two ad hoc design setup can be seen in section 5.4.

4.13 Registration GUI

A GUI was generated as a part of the project to present the results at Visiopharm. The interface of the GUI is presented in figure 4.33. A guide to use the GUI is presented in appendix B. The GUI software is attached as a CD in the appendix D. The GUI was very useful when demoing the results during the project to employees at Visiopharm.



Figure 4.33: Generated GUI for presenting the results to employees at Visio-pharm during the project.

4.14 Overview of the Fast Fourier Transform Based method

The FB rigid registration method is summarised to provide an overview of the different procedure. The FB registration method is based on 2D cross-correlation in the frequency domain to calculate the translation t . The rotation is estimated by transforming the images to a polar representation and using 2D cross-correlation in the frequency domain to calculate the rotational parameter \mathbf{R} . The 2D cross-correlation is modified to be weighted and limited to favour small transformation steps.

The FB registration method calculates the estimated registration as an iterative process. The deformation field is updated after each estimation of a rigid parameter yielding only one interpolation in the end. Zero padding is avoided by extracting a larger image that is applied the rigid transformation, to prevent a smaller Field of Views from being affected. The only pre-processing applied in the FB method is the transformation from RGB color images to gray-scale images.

CHAPTER 5

Results

This section contains the results obtained in this project. A study of the FB method is conducted on a 2D generated phantom to quantify the performance of the registration method. The results of a statistical analysis is conducted to compare The FB method to a manual Point Based registration and the registration results from Visiopharm's algorithm. The analysis is conducted on a randomly selected dataset. Furthermore a study was performed on the influence of detecting the rotation in whole degrees down to 1/16 of a degree.

5.1 Phantom

A difficult task in this project is to quantify the rigid registration of the real life medical images since the ground truth is unknown. The generated phantom displayed in figure 4.21 is used in attempt to quantify the performance of the algorithm generated in this project. The phantom is defined in values between 0 and 1. To simulate the rigid registration procedure, a set of 100 randomly selected translation parameters and rotation parameters are applied to the phantom to generate 100 registration scenarios. The randomly selected rotation parameters were from -10 to 10 degrees and were determined down to 0.01 degrees. The randomly selected translation parameters were between -50 and 50 with determined down to 0.1 pixel. To

evaluate the performance of the FB registration the Sum of Squared Difference is calculated for all 100 registration scenarios. The histogram of the SSD values calculated for the registrations are displayed in figure 5.1. To provide a comparison measure for the SSD values the mean SSD when the phantom is off by one pixel in each direction is given as a SSD value of 1075.

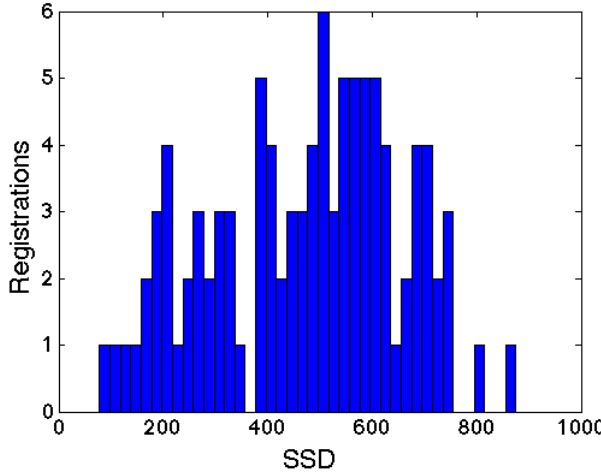


Figure 5.1: Histogram of SSD values calculated from 100 FB rigid registration conducted on the phantom in figure 4.21. The rotation and translation parameters were randomly selected and applied to the original phantom to generate registration scenarios used as input to the FB registration.

The mean of the SSD values in the histogram in figure 5.1 are calculated to 472.5 and spans from 78.1 to 874.9. It is noticed that there are no SSD values located far from the distribution seen in the histogram. There are seen no context in the SSD values and the simulated translation and rotation parameters. The result indicates that it is reasonable to proceed to registering tissue samples since the mean SSD value is below the mean SSD of a difference of one pixel.

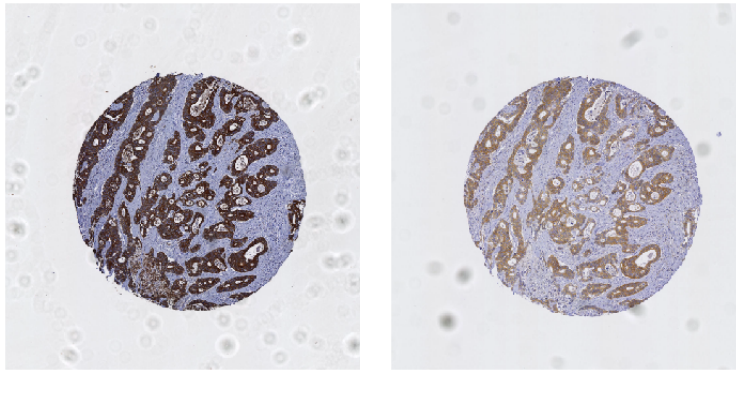
5.2 Dataset

The full dataset consists of 357 tissue samples. The tissue samples presented as TMA cores that are serial sliced. Each tissue sample is stained with three different types of antibodies e.g. PCK, Ki-67 and PHH3. To evaluate the FB

method, a representative sub dataset has been randomly selected between the 6 batches and the staining procedures. The extracted dataset consists of 50 tissue samples with two serial slices stained with two different antibodies. The random selection was performed with the MATLAB function `randi` and set to depend on the time.

Many of the procedures before the registration are manually performed e.g. extracting the biopsy, the slicing and staining of the tissue which all can inflict damages to the TMA cores. A description of distinct cores within the dataset are presented to understand the different challenges the FB registration is facing.

To begin the assessment of the challenges in the dataset an example core with minor challenges is presented for comparison in figure 5.2.

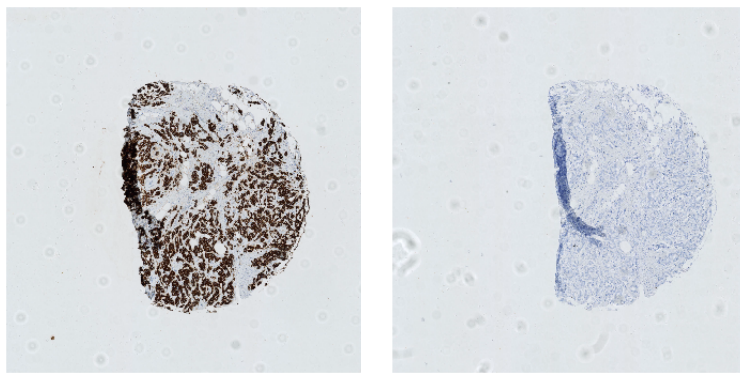


(a) Core stained with CK AE1AE3, I_1 (b) Core stained with erb-B2, I_2

Figure 5.2: Tissue sample number 5 of the randomly selected dataset. The cores are an example of detectable visual feature similarities. The antibody used for staining are (a) CK AE1AE3 and (b) erb-B2.

In figure 5.2 there are visible similarities in the main characteristics of the cores. One minor challenge could be that the core is close to circular, which could pose a challenge if the registration method chosen relies on the shape of the core.

One outcome of the manual preparation of the TMA cores could be that the tissue is folded or torn off. This could yield unwanted differences in intensities because of several layers of tissue and make it difficult for an automatic registration algorithm to estimate the optimal fit. An example of this is displayed in figure 5.3. Here the tissue samples are pushed together or folded at the left side. These folds could create intensity variations and variations in shape. These intensity variations could influence the registration.

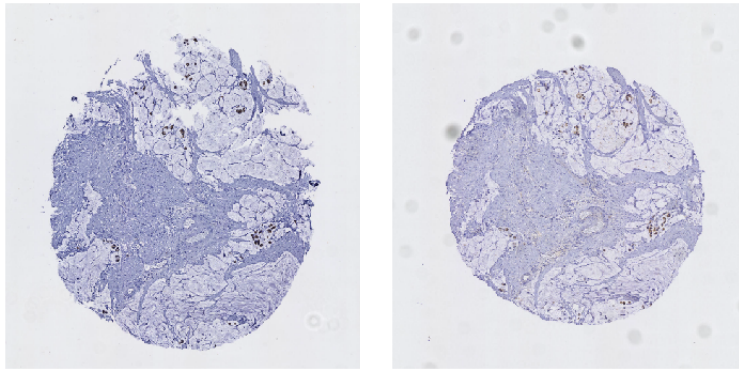


(a) Core stained with PCK, I_1

(b) Core stained with PHH3, I_2

Figure 5.3: Tissue sample number 24 of the randomly selected dataset. The cores are an example of manually induced challenges seen as folded or torn tissue. The antibody used for staining are (a) PCK and (b) PHH3.

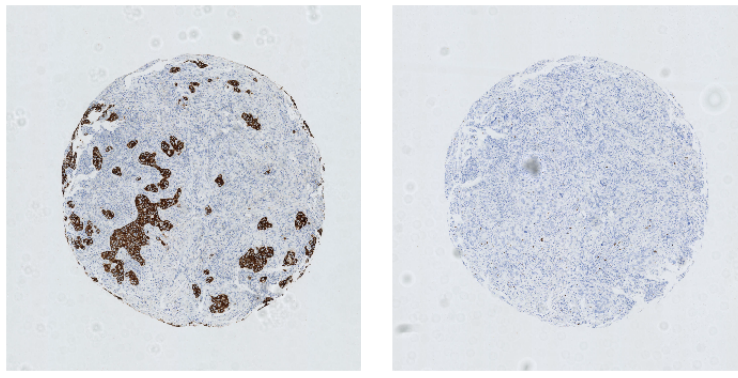
A result of the slicing could be a stretch in the tissue seen in figure 5.4(a). Here it looks like the e.g. microtome stretched the tissue at the top yielding different shapes of the cores. In this case, rigid transformation would not be sufficient for the complete optimal registration. The best guess for further non rigid registration could qualify as an optimal result.



(a) Core stained with CK AE1AE3, I_1 (b) Core stained with erb-B2, I_2

Figure 5.4: Tissue sample number 39 of the randomly selected dataset. The cores are an example of manually induced challenges seen as a stretch of the tissue. This could have been induced by the microtome. The antibody used for staining are (a) CK AE1AE3 and (b) erb-B2.

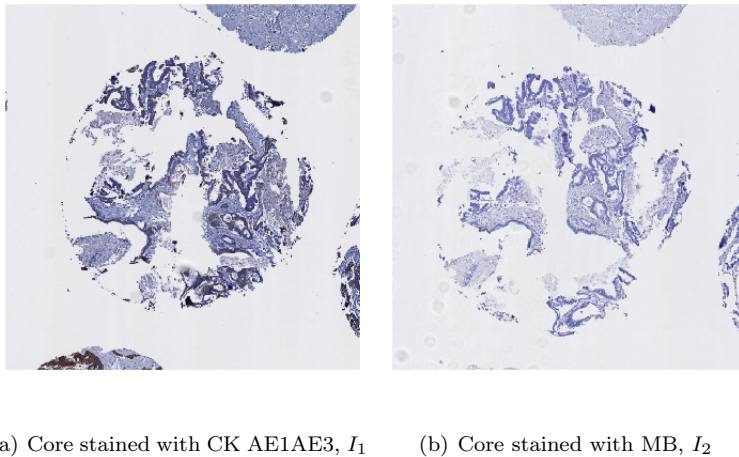
The PHH3 staining procedure is used to identify cells that are in a specific part of the cell cycle. This minimizes the visible information in the core after stain is applied. If the core is also round and have no large structures to recognize this could created difficulties for both an automatic registration and a manual registration. A tissue sample stained with PHH3 and no major characteristics is visualized in figure 5.5(b). The other staining procedure applied in figure 5.5(a) yields more features to base the registration on because of the PCK staining procedure.



(a) Core stained with PCK, I_1 (b) Core stained with PHH3, I_2

Figure 5.5: Tissue sample number 15 of the randomly selected dataset. a) Stained with PCK that presents large structures to recognize. b) Stained with PHH3 and an example of a uniform core with no major structure present and sparse of information from the PHH3 staining procedure.

A challenge where it is nearly impossible to estimate the optimal fit is presented in figure 5.6. When visually inspecting the cores it is difficult to locate similarities and this would probably also be difficult for a registration algorithm. The damage of the core have placed pieces very close to the other cores yielding difficulty in an automatic registration since they could influence the registration.



(a) Core stained with CK AE1AE3, I_1 (b) Core stained with MB, I_2

Figure 5.6: Tissue sample number 1 of the randomly selected dataset. The cores are an example of manually induced challenges seen as stretching and cracks in the tissue. This could have been induced by the microtome or other manual procedures. The core is also ripped so the pieces are very close to the surrounding core yielding difficulty in isolating the region of interest. The antibody used for staining are (a) CK AE1AE3 and (b) MIB.

The challenges visualized in the previous figures are a part of the randomly selected dataset. This representative dataset is used as input in the comparison of the manual PB registrations, the automatic FB registrations and Visiopharm's registrations. A statistical analysis is conducted in the following sections.

5.3 Manual placement of annotation points

The manually PB registration were conducted by a group of four test subject. The test group performed the PB registration with the GUI developed for this project described in section 4.11. Each subject were given the same instructions and were shown two test cores as an example. The test subjects were instructed to place four annotations points to locate similar structures in the images. They were all instructed to spread out the annotation point to minimize the error induced by small misplacements of the annotation points.

The largest distances are calculated in pixels between the 4 of the annotation points in each cores placed by the same test subject. The average of these distances for all test subjects are presented in table 5.1.

Table 5.1: Table of average maximum distance between annotation points for each test subject.

	Average maximum distance between annotation points
Test subject 1	382 pixels
Test subject 2	415 pixels
Test subject 3	430 pixels
Test subject 4	363 pixels

The mean diameter of the cores in the subset of tissue samples are approximately 500 pixels. The values in table 5.1 indicates that at least two of the annotation points placed by the test subjects are located around 400 pixels apart. This will minimize the error induced by small misplacements of the annotation points.

A timer were also implemented to study the time each test person took to annotate the four point in each registration. The average time of each test person is listed in table 5.2.

Table 5.2: Table of average time of placing annotation points for each test subject.

	Average time of placing annotation points
Test subject 1	27.6 sec
Test subject 2	41.4 sec
Test subject 3	63.8 sec
Test subject 4	52.5 sec

The average time of the manual Point Based registration gives an idea of the work load that it induces. The average time can be compared with the time it takes to perform FB registration on the same subset of cores. The annotation time and automatic computation time are discussed in section 6.5.

5.4 Statistical analysis of extracted dataset

The ad hoc statistical model setup in section 4.12 is used to give a quantitative evaluation of the results from the FB registration. In this analysis the main measures are the deformation field (Y) and Mutual Information.

5.5 Statistical analysis of the deformation field

The deformation field is used to evaluate the transformations performed by the manual PB registration and the automatic FB registration. Since the ground truth deformation field is unknown it is only reasonable to try to study if the deformation field of the FB method lies within the uncertainty of the PB deformation field generated by the test subjects. The study of the deformation field from equation 4.22 can be expressed as the following

$$\frac{\text{The difference in the deformation field from FB}}{\text{to the average deformation field from all the manual PB}} \\ \frac{\text{The uncertainty of the test groups deformation field}}$$

It should be noted that this is only an approximative analysis. The H_0 hypothesis is that the FB registration method is the same as the mean manual PB registration. The values obtained from this ad hoc analysis design are listed in table 5.3. The H_0 and H_1 hypothesis are listed below.

$$H_0 : Y_{FB} = \mu_{Y_{PB}}$$

$$H_1 : Y_{FB} \neq \mu_{Y_{PB}}$$

Table 5.3: Table of ad hoc statistical design values of deformation field comparison. A possible comparison could be the F -distribution at $F(0.05, 1, 3)$ equal to 10.13

core	ad hoc F-value	core	ad hoc F-value
1	0.6861	26	0.0253
2	0.5614	27	0.2621
3	0.2138	28	0.1412
4	0.0979	29	0.0640
5	0.3277	30	1.3195
6	0.1839	31	0.9153
7	0.1229	32	0.7031
8	0.2738	33	0.2289
9	0.0760	34	0.1658
10	0.1448	35	0.5017
11	6.7322	36	0.1015
12	0.2447	37	0.0304
13	0.8099	38	1.6128
14	0.6336	39	0.8153
15	0.5256	40	0.1981
16	1.3909	41	1.7983
17	0.0901	42	0.1337
18	1.1660	43	0.5715
19	6.5619	44	3.7571
20	0.8912	45	1.5857
21	0.2582	46	4.1578
22	0.2585	47	1.5806
23	0.2444	48	1.2735
24	126.6483	49	177.0866
25	1.0414	50	0.5016

The values from the ad hoc analysis are listed in table 5.3. To create a better overview, the data it is plotted as a histogram in figure 5.7. The F distribution is normally used in the analysis of variance to determine if the two test groups are significantly different from each other. The ad hoc statistical design is tried compared with the $F(0.05, 1, 3)$ value equal to 10.13, this value is also plotted in the histogram as a red line.

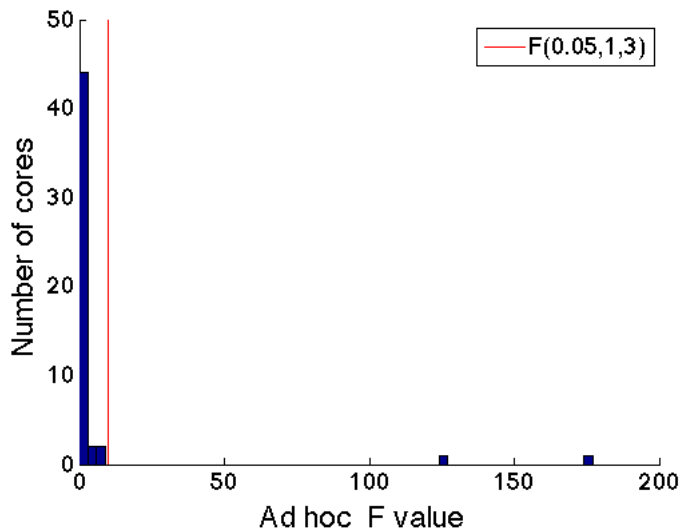


Figure 5.7: Histogram of the ad hoc analysis of the difference between the FB deformation field and the PB deformation field. The red line indicates the $F(0.05, 1, 3)$ value equal to 10.13.

When inspecting the histogram in figure 5.7 it can be seen that most of the registrations have values below the $F(0.05, 1, 3)$ value. Only two values in figure 5.7 are larger than $F(0.05, 1, 3)$. The cores with high values are core number 24 and core number 49. These two cores are inspected further to evaluate the reason for the high ad hoc F -value.

The registration of core number 24 is visualized in figure 5.8. Figure 5.8(a) is the registration result from the FB registration and figure 5.8(b) is the registration result from the PB registration of the average person. The registrations are visualized as half of each image separated by a red line. This visualization of the registered result gives an indication of how well the cores matches. The location of the separation line is individually selected from case to case.

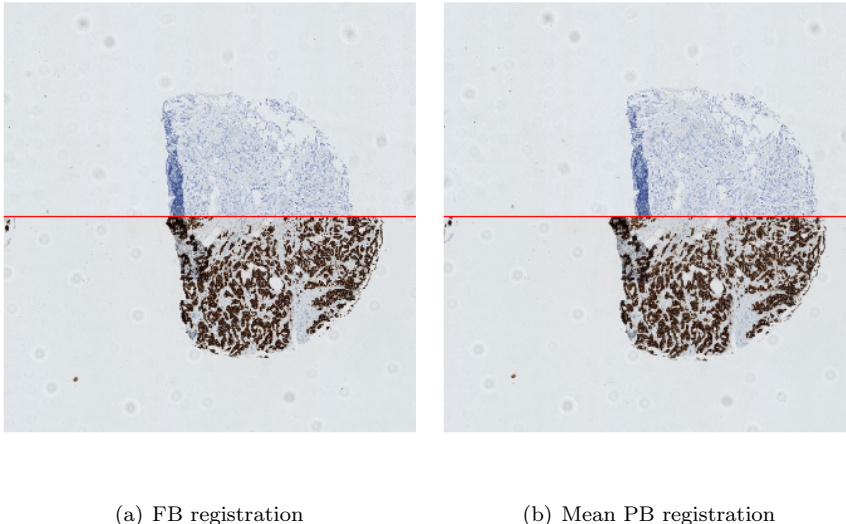


Figure 5.8: Tissue sample number 24 of the randomly selected dataset. The ad hoc F -value of this tissue sample was calculated to 126.6, stating that the two deformations fields estimated for the registration of this core is significantly different from each other. The core on the upper side of the red line is stained with PHH3 and the core on the lower side is stained with PCK.

It can be seen from the two registration results in figure 5.8 that the PB registration is different from the FB registration. The FB registration has fitted the cores to the left side where a fold is present. This could indicate that when a core is folded it can create troubles for the FB method. The PB registration is performed manually and if it is visible where the cores are similar it is less affected by a fold.

The registration of the second core with a larger ad hoc F -value than $F(0.05, 1, 3)$, is core number 49 which is visualized in figure 5.9. Figure 5.9(a) is the registration result from the FB registration and figure 5.9(b) is the registration result from the PB registration of the average person. The registrations are visualized as half of each image separated by a red line.

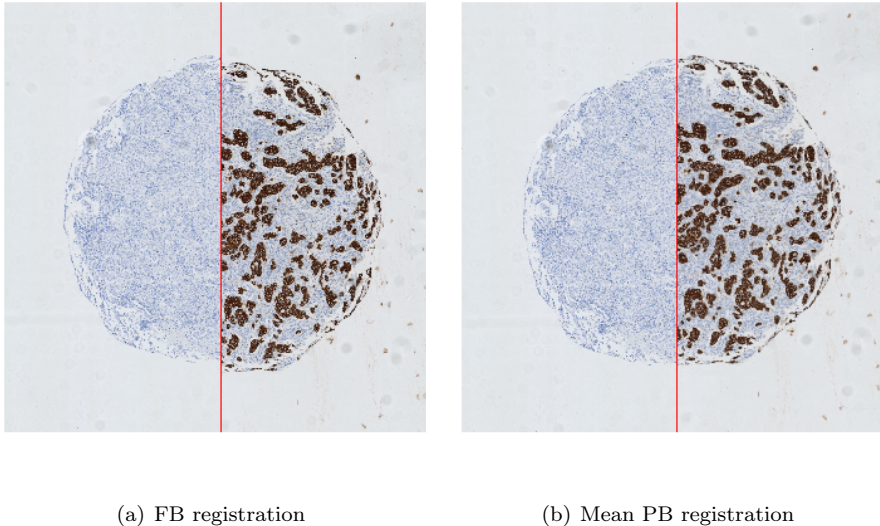


Figure 5.9: Tissue sample number 49 of the randomly selected dataset. The ad hoc F -value of this tissue sample was calculated to 177.08, stating that the two deformations fields estimated for the registration of this core is significantly different from each other. The core on the left side of the red line is stained with PHH3 and the core on the right side is stained with CK AE1:AE3

Core number 49 that is presented in figure 5.9 has the same characteristics as the challenging core presented in figure 5.5 section 5.2. Here the core to the left of the red line has sparse recognizable characteristics compared to the right. The FB registration in figure 5.9(a) has translated the left core a little higher than the PB registration in figure 5.9(b). This could be what influenced the large ad hoc F -value.

The remaining 48 registered cores in dataset were seen to have ad hoc F -values lower than $F(0.05, 1, 3)$. The H_0 hypothesis could not be rejected for these cores based on the ad hoc F -value. These cores represent 96 % of the randomly selected subset.

5.6 Statistical analysis of similarity measure

One of the goals of this project was to generate a rigid registration method that performed better than the already existing algorithm implemented in Visiopharm's software. Since the deformation field from Visiopharm's registrations were unavailable at this point the similarity measure MI is used instead. The ad hoc analysis for comparing the registration results from to algorithms was presented in section 4.12. The value of comparison is now reduced to a scalar unlike the deformation field. The ad hoc statistical design setup from equation 4.24 can be described as the following

$$\frac{\text{The difference in MI between the FB registration and Visiopharm's registration}}{\text{The uncertainty of measured MI within the test group}}$$

It should be noted that this is only an approximative analysis. If it is assume that MI is a valid quality measure of the registration between mamma cancer tissue samples, then the sign of the ad hoc t-value would give an indication of which one has a better fit. The H_0 hypothesis is that the FB registration is equal to the registration obtained by Visipharm's algorithm. The ad hoc t-values are presented in table 5.4 and the H_0 and H_1 hypothesis are listed below.

$$H_0 : MI_{FB} = MI_{VIS}$$

$$H_1 : MI_{FB} \neq MI_{PB}$$

Table 5.4: Table of ad hoc statistical design values of MI comparison between Visiopharm's registration results and the results obtained by the FB registration.

core	ad hoc t-value	core	ad hoc t-value
1	5.2198	26	12.4071
2	10.9903	27	0.3879
3	16.2666	28	-2.9490
4	2.8902	29	12.7257
5	2.9708	30	1.4413
6	4.9808	31	3.3435
7	3.9695	32	1.2133
8	1.4426	33	1.6272
9	0.5743	34	3.0202
10	7.7668	35	4.4123
11	6.9382	36	6.5783
12	2.2628	37	3.0012
13	6.2389	38	-4.7383
14	0.3096	39	5.6878
15	1.4689	40	4.6075
16	0.9265	41	0.3340
17	3.0861	42	9.7341
18	8.6539	43	1.4893
19	26.0051	44	1.8986
20	1.7496	45	2.0298
21	12.5479	46	8.7738
22	3.5991	47	0.3007
23	0.7095	48	1.7597
24	-2.4083	49	-0.4984
25	1.8066	50	2.2131

An overview of the ad hoc t-values are given as a histogram in figure 5.10. The t-distribution is normally used to state if the hypothesis can be rejected. The ad hoc approximate analysis is attempted to be compared with the t-value at three degrees of freedom and an α of 0.05 this is equal to $t(0.05/2, 3) = 3.182$. The $\pm t$ -value is displayed in the histogram as red lines.

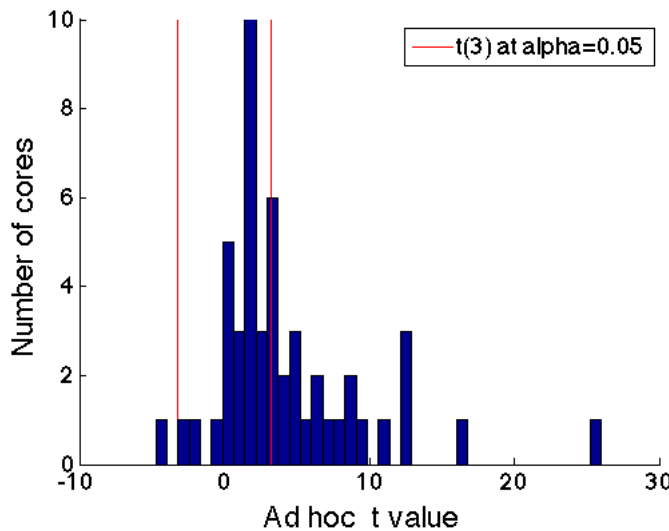
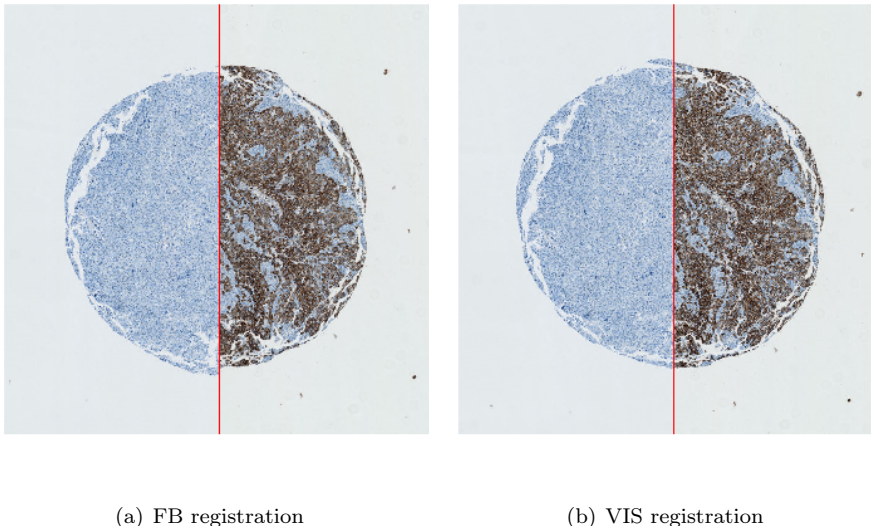


Figure 5.10: Histogram of the ad hoc analysis of the Mutual information of the FB and VIS registration. The red line indicates the t-value at 3 degrees of freedom and an α of 0.05 equal to $\pm t(0.05/2, 3) = \pm 3.182$

Several ad hoc t-values from the registrations, states that the registration between the FB registration and Visiopharm's registration is significantly different from each other. The sign in front of the ad hoc t-value indicates where the FB registration has a higher MI than Visiopharm's registration. If the ad hoc t-value is positive the FB registration has a higher MI than Visiopharm's registration.

Four cores have negative ad hoc t-values and one of them are stated to be significantly different from Visiopharm's registration. The core with the lowest value is visualized in figure 5.11.



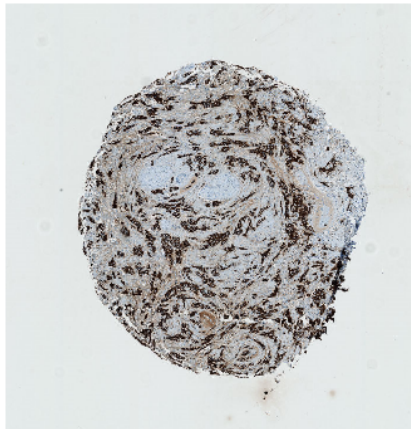
(a) FB registration

(b) VIS registration

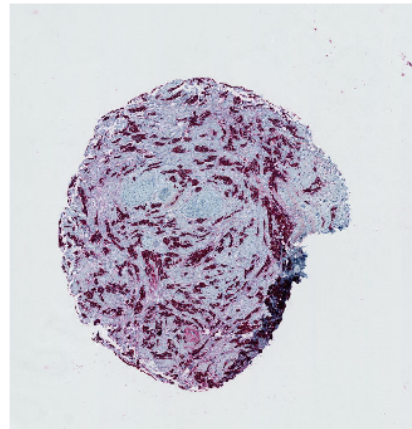
Figure 5.11: Tissue sample number 38 of the randomly selected dataset. The ad hoc t-value of this tissue sample was calculated to -4.7383, stating that the calculated MI's for the registrations of this core are significantly different from each other at a t-value of three degrees of freedom and an α of 0.05 equal to $\pm t(0.05/2, 3) = \pm 3.182$. The sign in front of the t-value indicates that Visiopharm's registration has a higher Mutual Information. Left of the red line is stained with ER. Right of the red line is stained with PCK.

In figure 5.11 it is noted that core number 38 has the same characteristics as the core in figure 5.5. The information is sparse in the core on the left stained with ER this yields problems for the FB registration method. The sign in front of the t-value indicates that Visiopharm's registration has a higher Mutual Information than the FB method.

Core number 28 has an ad hoc t-value of -2.9490. The registration of the FB method and Visiopharm's method can not be determined significantly different from each other but the value indicates that Visiopharm's registration is better based on MI. The cores are visualized in figure 5.12 before performing any registration to inspect the cores of possible challenges.



(a) Core 28, stained with PCK



(b) Core 28, stained with ER-PCK

Figure 5.12: The original tissue sample number 28 of the randomly selected dataset. The cores are visualized with before performing any registration to inspect the cores of possible challenges.

When inspecting the cores it can be seen that there is a fold in the lower right region in figure 5.12(b). The registrations are attempted visualized in figure 5.13.

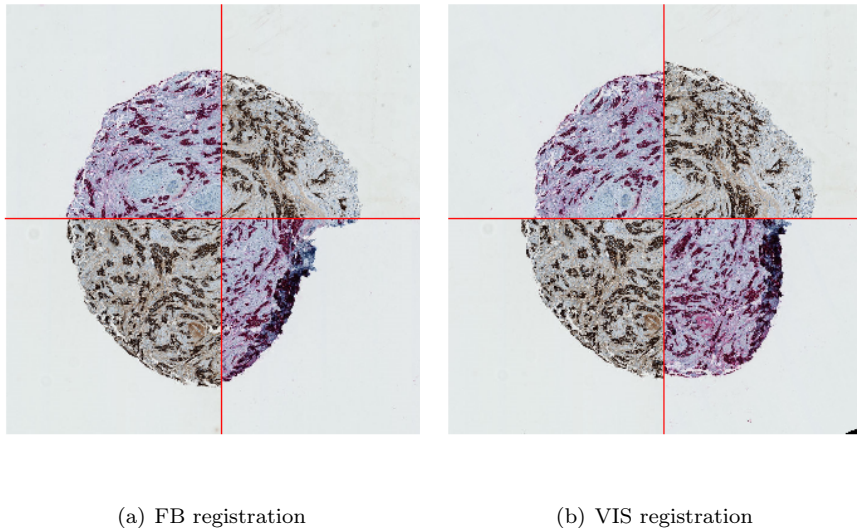


Figure 5.13: Tissue sample number 28 of the randomly selected dataset. The ad hoc t-value of this tissue sample was calculated to -2.9490, stating that the calculated MI's for the registrations of this core are **not** significantly different from each other at a t-value of three degrees of freedom and an α of 0.05 equal to $\pm t(0.05/2, 3) = \pm 3.182$. The sign in front of the t-value indicates that Visiopharm's registration has a higher MI.

The registration of core 28 for the FB registration and Visiopharm's registration are given in figure 5.13. It is noted that Visiopharm's registration yielded a higher MI than the FB registration, but when visually inspecting VIS registration it can be seen that the core is rotated far more than expected from the original images visualized in figure 5.12. The FB registration is seen to have accounted for the fold.

The registration of the core 3 that has the highest ad hoc t-value is visualized in figure 5.14. The ad hoc t-value calculated for this core is 16.2666, indicating that the two registrations from FB and VIS are significantly different from each other. The sign of the ad hoc t-value indicates that the FB registration has a higher MI value than Visiopharm's registration.

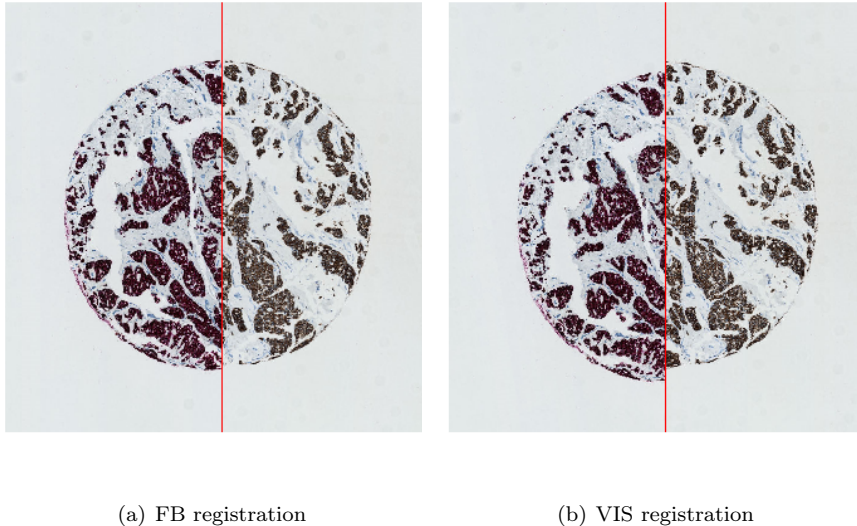


Figure 5.14: Tissue sample number 3 of the randomly selected dataset. The ad hoc t-value of this tissue sample was calculated to 16.26, stating that the calculated MI's for the registrations of this core are significantly different from each other at a t-value of three degrees of freedom and an α of 0.05 equal to $\pm t(0.05/2, 3) = \pm 3.182$. The sign in front of the t-value indicates that the FB registration has a higher MI.

The registrations of core number 3 reveals that the registration from VIS is off, as expected from the sign of the t-value. The registration from FB is seen to be aligned at the edges unlike the registration from VIS.

The same ad hoc analysis that is based on MI can be applied to the PB registration. The difference between the MI of the FB registration and the mean MI of the PB registrations can provide an indication of the registration quality unlike the deformation field. The ad hoc t-values from the comparison of the FB registrations and the mean PB registration is listed in table 5.5.

$$H_0 : MI_{FB} = \mu_{MI_{PB}}$$

$$H_1 : MI_{FB} \neq \mu_{MI_{PB}}$$

Table 5.5: Table of ad hoc statistical design values of Mutual Information comparison between the mean MI of the test group and the MI obtained by The FB registration.

core	ad hoc t-value	core	ad hoc t-value
1	0.7020	26	1.5007
2	1.2996	27	1.9628
3	1.2465	28	0.8967
4	1.2190	29	2.4679
5	1.4623	30	1.3777
6	4.6998	31	1.1701
7	2.0455	32	2.0731
8	2.0045	33	1.5809
9	1.0878	34	2.0834
10	1.7690	35	1.1964
11	6.9095	36	2.2106
12	1.5788	37	2.5519
13	-0.6279	38	-2.3097
14	0.4700	39	0.4516
15	1.7042	40	1.3564
16	1.6865	41	1.5961
17	1.7093	42	1.3267
18	0.8885	43	0.9014
19	1.4109	44	0.5003
20	1.4135	45	0.0824
21	0.6475	46	1.1092
22	2.2284	47	-0.8539
23	0.8266	48	0.7954
24	-3.7594	49	-9.4600
25	0.4450	50	1.0975

The overview of the ad hoc t-values are presented as a histogram in figure 5.15. The ad hoc approximate analysis is attempted to be compared with the t-value at three degrees of freedom and an α of 0.05 equal to $\pm t(0.05/2, 3) = \pm 3.182$. The \pm t-value is shown in the histogram as red lines.

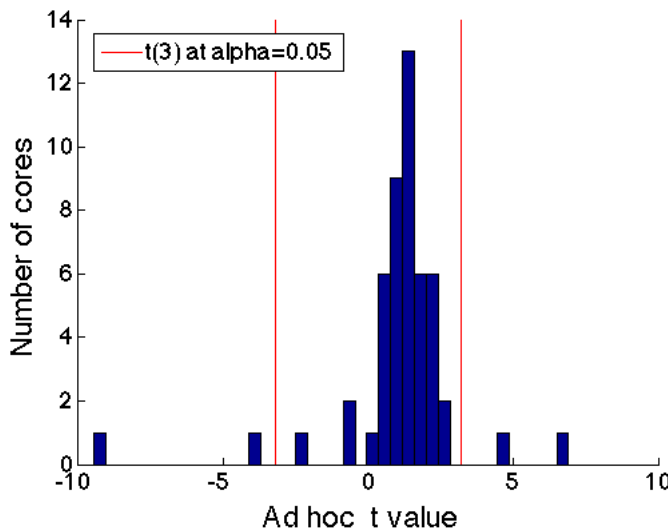
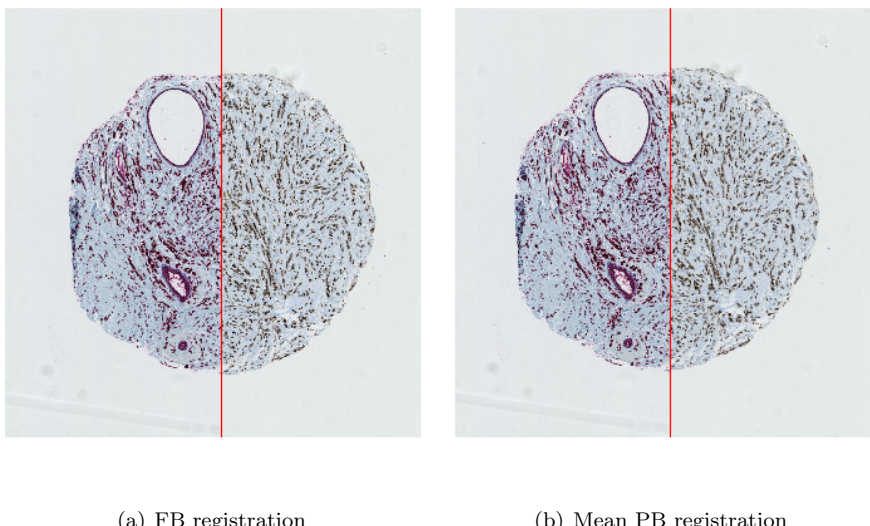


Figure 5.15: Histogram of the ad hoc t-values from analysis of the MI of the FB registration and the PB registration. The red line indicates a t-value of three degrees of freedom and an α of 0.05 equal to $\pm t(0.05/2, 3) = \pm 3.182$

The two registrations that have a negative ad hoc t-values and are significantly different is core number 24 and 49, which also were stated significantly different in the ad hoc statistical analysis of the deformation field in section 5.5. The two registrations that have a positive ad hoc t-values and are significantly different is core number 6 and 11. The two registrations are attempted visualized in figure 5.16 and 5.17.



(a) FB registration

(b) Mean PB registration

Figure 5.16: Tissue sample number 6 of the randomly selected dataset. The ad hoc t-value of this tissue sample was calculated to 4.6998, stating that the calculated MI's for the registrations of this core are significantly different from each other at a t-value of three degrees of freedom and an α of 0.05 equal to $\pm t(0.05/2, 3) = \pm 3.182$. The sign in front of the t-value indicates that the FB registration has a higher MI than the PB registration.

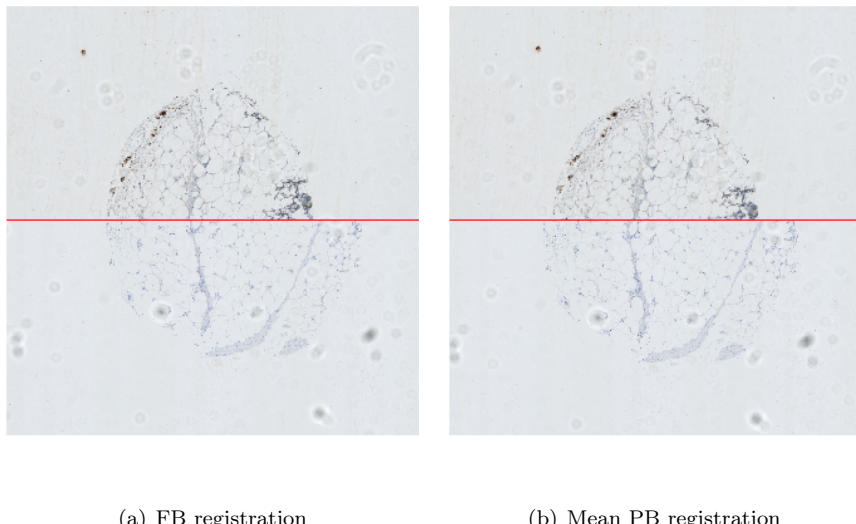


Figure 5.17: Tissue sample number 11 of the randomly selected dataset. The ad hoc t-value of this tissue sample was calculated to 6.9095, stating that the calculated MI's for the registrations of this core are significantly different from each other at a t-value of three degrees of freedom and an α of 0.05 equal to $\pm t(0.05/2, 3) = \pm 3.182$. The sign in front of the t-value indicates that the FB registration has a higher MI than the PB registration.

It is difficult to visually determine the difference of the two registration in figure 5.16 and 5.17. If the cores are visualized as an overlay in MATLAB where they are switched between the difference is noticeable. The registration can be visualized with the GUI generated for demonstration.

5.7 Rotation study

A study of the estimation of the angle θ in the rotation parameter is conducted. The estimation of degrees of rotation in the FB registration method is bound to the number of wheel spokes in the polar representation described in section 4.5.2. The wheel spoke frequency determine how small an angle that can be detected. Different values wheel spoke frequencies are listed in table 5.6 and implemented. The rotation study is also based on the assumption that MI is a good measure to determine the quality of the fit. The mean computation time is also listed.

Table 5.6: Table of wheel spoke frequency study

Degrees detectable	Mean MI value of the 50 cores	Mean time
1 wheel spoke per degree	0.6768	2.36
2 wheel spokes per degree	0.6820	3.32
4 wheel spokes per degree	0.6866	4.46 sec
8 wheel spokes per degree	0.6891	7.44 sec
16 wheel spokes per degree	0.6887	15.98 sec

In table 5.6 the average MI values are observed to increase a little with the increase in wheel spokes frequency of the the polar representation. The mean MI has increased 0.0123 from 1 to 8 wheel spokes per degree. The maximum increase in MI of one registration is 0.103 this is when going from 1 to 8 wheel spokes per degree. The maximum was detected in the registration of tissue sample number 15 and is an increase of 15.9 % of the original MI value.

CHAPTER 6

Discussion

This chapter contains a discussion regarding the results presented in chapter 5. The discussion revolves around the project definition which were to generate a rigid registration method for registration of TMA microscopy based image. The method were to be computational efficient for possible commercial use.

6.1 Phantom

In an attempt to make a quantification of the FB registration method, a series of 100 randomly selected translation parameters and rotation parameter were applied to the phantom displayed in section 4.9. A registration were then calculated, with the original phantom as the reference image I_1 and the rotated and translated version of the phantom as the image to transform I_p . The result of the registrations were evaluated by calculating the SSD between image I_1 and image I_p , where p denotes the randomly selected translation and rotation parameter. The images were of value from 0-1 and and a size of 700x700 pixels. The optimal result would be to have a SSD value of zero.

The mean SSD value of the 100 rigid registrations scenarios created was 472.5. For comparison SSD value 1075 is given which reflects the mean SSD when translating the phantom one pixel in each direction. In the comparison it is

seen that the mean difference is less than one pixel. The value are not zero which states that the registrations were not perfectly aligned. It should be noticed that a SSD value of zero is hard to obtain because the precision limitation in the FB registration. The purpose of the phantom analysis is to verify the the results of the rigid registrations before applying it to the microscopic mamma tissue images. The study could also reveal if the algorithm had difficulties with certain estimations such as large degrees or small translations. When inspecting the histogram in figure 5.1 there are no noticeable outliers. Furthermore, there seems to be no connection between the different rigid parameter applied to the phantom and the SSD values. The SSD value might be affected by the interpolation that occurs when applying the registration and yield an error that is difficult to prevent.

The result from the phantom study states that the mean error is under one pixel and proceeding to real mamma tissue is reasonable. Furthermore there were no indications that the FB method had weaknesses connected to the values of the translation or rotation parameters.

6.2 Manual Point Based registration

The manual registration chosen for comparison were a PB registration estimating a translation and a rotation based on 4 annotation points. The annotation points were place by four test subjects. The annotation points were placed with good separation between them listed in table 5.1. The GUI for placing the annotation were developed to be simple for the users. Various features could have been implemented such as zoom to place the annotation points, but the dataset was limited to only one magnification setting and could not be changed at this point. A zoomed field of view could have increased the accuracy of placing the annotation points.

6.3 Statistical analysis

An ad hoc statistical analysis of 50 randomly selected tissue samples from a dataset of 357 tissue samples were conducted to present a statistical evaluation of the FB registration method. The FB registration method were compare with a manual PB registration based on four annotation points placed by four test subject. These PB registrations of the 50 randomly selected cores formed the basis of the ad hoc statistical analysis.

A comparison of the deformation fields from the average test subject and the deformation fields from the FB registration were conducted. The results showed that 96 % of the registrations could not be determined significantly different from each other based on the deformation field. Two of the registrations turned out to be significantly different based on the ad hoc statistical analysis of the deformation field. They both had features similar to challenging cores described in the review of the dataset in section 5.2.

The TMA core number 24 was observed to have a fold in the left side of the tissue. This fold could have led to the significantly different deformation field compared to the manually PB deformation field. When visually inspecting the registration in figure 5.8 it was noticed that the registration could have failed because of the intensity difference created by the fold along the edge.

The other registration that had a significantly different deformation field based on the ad hoc statistical analysis was TMA core number 49. The staining procedures of the cores were PCK and PHH3. The PHH3 staining procedure singles out cells in a specific part of the mitosis and is usually faint because of the specific marking. The faint PHH3 marking does not create new features to register by and the tissue in the core is noticed to be very uniform without major characteristics. The combination of the faint marking and the lack of characteristics in the tissue could be what resulted in the significantly different deformation fields.

An ad hoc statistical analysis was also conducted based on the similarity measure Mutual Information. If MI is assumed to depict the quality of the alignment, MI could serve as a quantitative measure. Mutual Information from the FB registrations, PB registrations and the registrations performed by Visiopharm's algorithm were compared with the ad hoc statistical analysis.

The results from the statistical analysis between Visiopharm's registrations and the FB registrations are listed below.

- 42 % of the FB registrations had a higher calculated MI than Visiopharm's registration, and were significantly different from each other according to the ad hoc statistical analysis.
- 2 % of Visiopharm's registration had a higher calculated MI than the FB registrations, and were significantly different from each other according to the ad hoc statistical analysis.
- 92 % of the FB registrations had a higher MI than Visiopharm's registrations.

The results from the ad hoc statistical analysis of the subset showed that the FB method performed better when compared to the existing algorithm in Visiopharm's software. The improvement of 92% of the registrations indicates that Visiopharm could benefit from implementing the FB registration method in their software.

The registration where Visiopharm had a higher calculated MI were of a serial sliced core where the marking from the staining procedure was faint. The same result was seen in the registration of core number 49, with the manual PB registration. Further more when inspecting the core it was noticed that the core stained with ER had no apparent holes or large structures to based the registration on. This could indicate that if there is a lack of information from the staining process and the structures are very uniform in one of the tissue samples the FB algorithm has trouble estimating the right alignment.

The FB registration result from the cores containing folds were not conclusive. The results from registration number 28 displayed in figure 5.13 showed that the FB registration made a good estimation of the alignment, despite the fold present in the core. The ad hoc t-value were calculated to 0.8967 when comparing the Mutual Information from the FB method and the PB method in table 5.5. The positive value states that the FB registration were better based on MI, but not significantly.

Another example of a core with a fold were registration number 24. Here the PB registration were better than the FB registration which is displayed in figure 5.8. The results of the folded core number 24 could indicate that manual PB registration is more robust than the FB method when aligning cores with fold or damages. This applies if the cores still have recognizable structures. The FB registration method can be misled by the damages inflicted on the tissue samples.

From the comparison between the FB method and the PB method in histogram in figure 5.15 it can be seen that most of the value are located on the positive side. This indicates that the FB registration method is better, although when looking at the significance only two of the ad hoc t-values states significant difference between the two registration methods. If the result was based only on MI then 90 % of the FB registrations have a higher Mutual information than the mean manual PB registration.

To compare the entire dataset the MI for all cores are calculated with the FB algorithm and with Visiopharm's algorithm. The total performance just based on Mutual Information and no statistical analysis, is displayed in appendix C figure C.1. The comparison shows that 92.7% of the FB registrations has a better MI than Visiopharm's registration and the mean improvement of MI

was 12.5 %. This result resembles the result from the statistical analysis of the sub dataset.

The statistical analyses conducted in this project were generated to fit this particular design of experiment. The approximative results are compared with known statistical distributions as the F -distribution and the t-distribution yielding approximative conclusions. Further statistical designs could be generated to expand the analysis. A group of pathologist could be included to score the FB registration to get a qualified professional opinion of the result from the FB registrations.

6.4 Rotational Study

The estimation of the rotation parameter \mathbf{R} is highly influenced by the wheel spoke frequency. A study of different wheel spokes frequency values was conducted and presented in section 5.7. The study went from sampling one wheel spoke per degree to 16 wheel spoke per degree. The similarity measure collected from the study were Mutual Information, if it is assumed that this is a good measure of the alignment then it indicates the development of the registration in the study.

The mean MI of the 50 randomly selected tissue samples were collected at the different wheel spokes frequencies. The mean MI value was seen to increase with the increase in wheel spoke frequency. This could indicate that the relation in rotation between two cores are estimated with higher precise in the rotation estimation. When implementing a degree estimation with 16 wheel spokes per degree, the mean MI value began to lower compared to sampling with 8 wheel spokes per degree. The lowering of the mean MI could be the result of an oversampling of the images when generating the polar representation.

In the statistical analysis 8 wheel spokes per degree where used in the polar representation to estimate the angle θ in the rotation parameter \mathbf{R} .

6.5 Computation time

The computation time is important when implementing the rigid registration method for commercial use. A part of the project definition were to make the

rigid registration method computational efficient. The FB registration uses Fourier Transformation as the main operator in the registration which is a highly computational efficient calculation. Other operations within the algorithm could also influence the computation time, such as the generation of the polar representation.

The mean computation time changes when the wheel spoke frequency is increased. This is listed in the rotation study in table 5.6 section 5.7. The average time of the registrations increased from 2.36 sec to 15.98 sec when calculating the polar representation with one wheel spoke per degree to 16 wheel spoke per degree. The MI formation seemed to increase as well and this states that the computation time is connected to the quality of the registration. The MI were seen to decrease a little when having a wheel spoke frequency of 16 wheel spoke per degree. This could indicate that there is a limit of available information in a given image size. A further increase of the wheel spoke frequency would increase the computation time but not improve the result.

The manual PB registration were timed to compared with the automatic FB registration method. The average time of the four test subject for one registration were 46.3 seconds compare to 7.4 seconds for the FB registration method. The manual registration time and result could be influenced by the time of day, work load and experience. This is compared to the FB registration method that performs the same each time and yields the same result independent of the operator if the guidelines in section 4.2 are followed.

The FB registration method were implemented in MATLAB and executed on the computer listed in appendix A.1. The computation time is expected to decrease significantly if the FB registration method is implemented in C.

6.6 Method

The FB rigid registration method implemented and modified in this thesis has proven to be highly usable when performing rigid registration on microscopic images of TMA cores of breast tissue. The 2D cross-correlation in the Fourier space showed to use the information in the different structure of the tissue sample even though they were not completely identical.

Beneficial changes implemented could be an initial guess of the rotational point. In the FB registration method the rotational point is estimated as an iterative process and could benefit from a robust initial guess. The improved initial guess could decrease the number of iterations and possibly yield a lower

computation time. A robust tissue segmentation method were not developed for this project because of the various challenging cores present in the dataset. An example of a core that imposes a challenge is core number 11 visualized in figure 5.17. In this example it is difficult to determine the tissue from the background which could led to a wrong tissue detection and a poor initial guess. Other challenges such as ripped cores and variations in staining could also cause difficulties when performing tissue segmentation.

There could have been implemented a zoom function to register a smaller field of view to align tissue that had been torn or stretched. This would have demanded a microscopic image of a higher magnification to present the new field of view in a higher resolution.

6.7 Pre-processing

A set of pre-processing procedure were implemented to see if they improved the registration. An attempt to equalize the differences in the tissue which are introduced by using different types of stains was conducted. None of the chosen pre-processes and variables showed overall improvements on the rigid registration. The Gabor filter resulted in an increase in the number of iterations used to estimate the rigid parameters with the FB method and did not yield a higher MI. When using the frequency domain based cross-correlation to estimate the rigid parameters the selected edge detection did not yield any improvement. It was noticed that some cores in the dataset had small scale differences, possible due to the different staining procedures. This could influence the registration of the detected edges and a scale parameter estimation might be beneficial when using the Gabor filter.

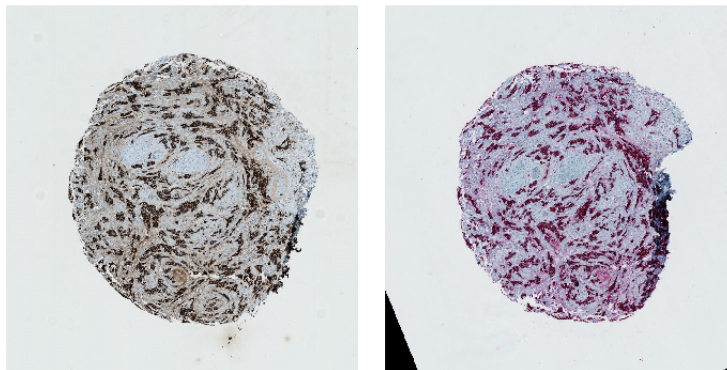
The Chromaticity was implemented in an attempt to equalize the intensity inflicted by the staining procedure. The chromaticities were calculated for each colorband and tested at across each combination of for the different staining procedures presented in the dataset. The test did not reveal a beneficial combinations of the chromaticities calculated before registration with the FB registration method. The chromaticity also yielded an increase in iterations indicating troubles with estimating an alignment.

It is likely that an unknown pre-processing could improve the result, but is yet to be found.

6.8 Similarity measure

Mutual Information is assumed to reflect the quality of the rigid registrations conducted in this project. The visual inspection of the results seems to verify this assumption in most cases of the registrations in this report. But this assumption is only valid if there are recognisable similarities between the images. The Mutual Information only expected to reflect the quality of the alignment if an alignment is possible.

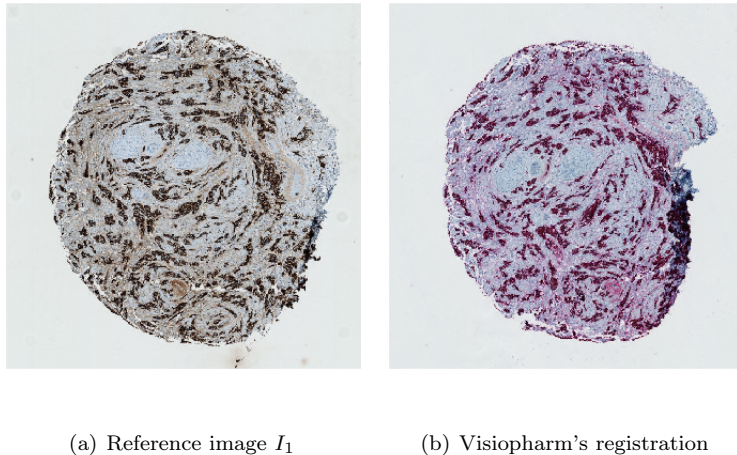
In registration number 28 where one of the cores had a folded or missing piece of tissue then it showed that it was possible to obtain a higher mutual information that did not reflect the best fit seen in figure 5.13. When studying the registration from Visiopharm shown in figure 6.1, it can be seen that there are zero padding present within the Field of View. This zero-padding could affect the calculation of the MI. To try and test this the FoV is made smaller and visualized in figure 6.2



(a) Reference image I_1

(b) Visiopharm's registration

Figure 6.1: Visiopharm's registration of tissue sample number 28 of the randomly selected dataset.

(a) Reference image I_1

(b) Visiopharm's registration

Figure 6.2: Visiopharm's registration of tissue sample number 28 of the randomly selected dataset. The Field of View has been reduced compared to the original registration showed in figure 6.1 to discard the zero padding before calculating the MI.

The calculated Mutual Information now states the the FB registration has the highest MI, indicating that it has the best alignment. The ad hoc t -value for registration number 28 is now 9.80 stating that the two registrations are significantly different from each other and the FB registration has the best estimated fit.

This reduction in FoV could indicate the needs for a good robust tissue segmentation algorithm, so only the tissue of interest is used in the calculation of the MI. This would enhance the use of Mutual Information as the similarity measure.

CHAPTER 7

Conclusion

An automatic iterative rigid registration method were developed and modified in this project. The method were based on cross-correlation in the frequency domain to estimate the translation and the rotation. The Fourier Transformation was executed with Fast Fourier Transform. A weighting and a limitation was implemented to favour small steps in the estimation. The Fast Fourier Transform based (FB) method was compared with a Point Based (PB) rigid registration. The PB registration was conducted by a group of four test subjects that each placed four annotation points in a developed GUI. A representative subset of randomly selected tissue samples were used for the statistical the analysis. 96% of deformation fields from the manual PB registration and the FB registrations could not be determined significantly different from each other. The study was based on an adapted statistical analysis that resembled a F-test with (1,3) degrees of freedom at an α of 0.05.

A second adapted statistical analysis, based on the similarity measure Mutual Information, was conducted to compare the FB registrations with Visiopharm's registration results. The ad hoc statistical analysis showed that 42% of the registrations were significantly different from each other, where the FB registrations had the highest Mutual Information indicating a better alignment. 92% of the FB registrations resulted in a better Mutual Information than the existing algorithm in Visiopharm's software. The Mutual Information based comparison between the manual PB method and the FB

method, stated that in 90 % of the FB registrations had a higher Mutual Information than the PB registrations.

The statistical analysis of the FB method revealed that cores with certain characteristics are difficult to align. The characteristics of the cores are faint marking from the staining procedure, combined with uniform structures and a lack of recognizable features such as holes. These type of cores does not form the majority of the biopsies in the dataset, but will have to be studied further to find a solution.

Since the true rigid registration is unknown it is recommended that the tissue alignment results are manually review by a pathologist when used for diagnostics.

Perspective

Further statistical analysis could be to get a team of pathologists to perform a scoring of the registrations to have a qualified professional opinion of the optimal registration result. The results from the pathologists could be compared to the Mutual Information score and determine if the assumption is correct.

Additions to the FB method could be to implement a robust segmentation of the tissue. This could be used to determine the rotational center and then provide a solid initial guess before registration. The segmentation could also be used in the Mutual Information calculation to reduce the background noise. A scale estimation could also be implemented to account for the scale variations that are noticed in the dataset.

APPENDIX A

Computer specs.

Table A.1: Computer description

Description of the computer used in project	
Manufacturer	Apple
Processor	2.53 GHz Intel core 2 duo
RAM	8 GB 1067 MHz DDR3
OS	Mac OS X v. 10.7.5
MATLAB version	8.0.0.783 (R2012b)

APPENDIX B

Registration GUI demo

A GUI was generated as a part of this project to present the registration result of the different TMA cores.

This section contains a user guide that describes the different steps in the GUI. The rigid registration method used in the GUI is the one described in this thesis. The GUI is presented in figure B.1.

The GUI can be opened in MATLAB from the first folder of the attached CD.

The first step is to select a dataset in the listbox in the top of the tool bar at the right side of the GUI displayed in figure B.1.



Figure B.1

Then pick a core from the overview image with the cursor. The core now appears in the field of view displayed in figure B.2. To choose the next core click the Next core button. The registration method is set to FB registration. Then choose a staining type to align with from the fourth listbox in the tool bar to the right.

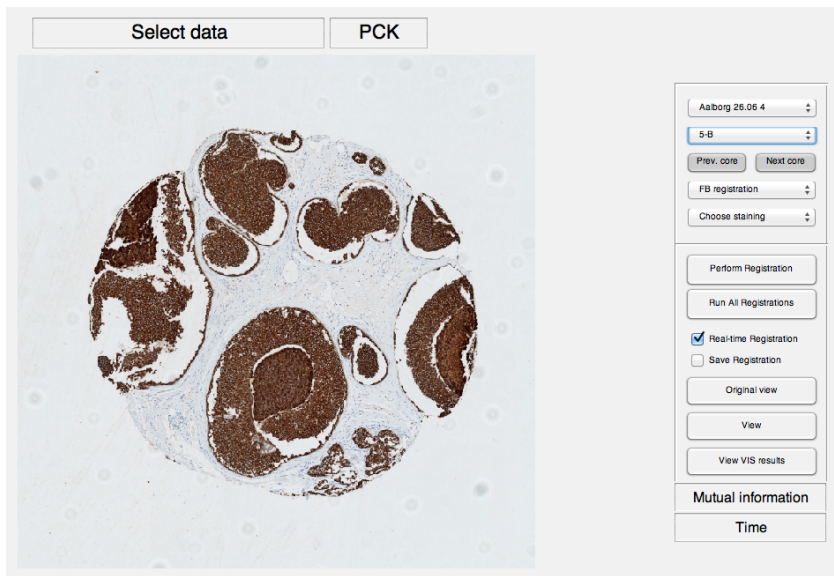


Figure B.2

The the rigid registration is initiated by clicking Perform Registration. The result is then displayed in the figure and the two cores can be switched between by tapping view. A finished registration is displayed in figure B.3.



Figure B.3

The original image can be switch between by clicking Original view and the result from Visiopharm's registration can be view by clicking view VIS results.

The Mutual Information is displayed together with the calculation time and the registration result can be saved by checking Save Registration.

To speed up demonstrations the saved images can be showed faster than the real registration. The Real-time registration check box can be marked and the registration is performed in real time.

The GUI was very useful when demoing the results to employees at Visiopharm during the project.

APPENDIX C

Full dataset comparison

A comparison between registrations of all the cores in the dataset is displayed in this section. The comparison is based on Mutual Information and is between the FB registrations and Visiopharm's registrations. The comparison is displayed in figure C.1. This comparison resembles the result obtained in the statistical analysis.

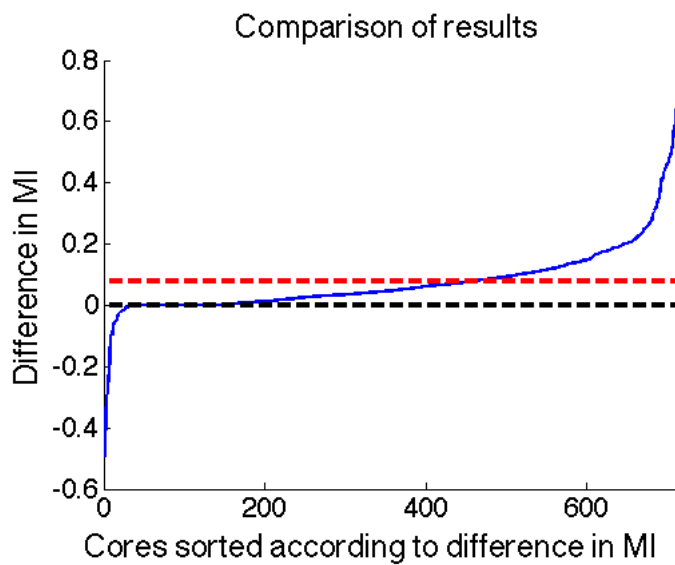


Figure C.1: Difference in Mutual Information between the FB registrations and Visiopharm's registrations of the entire dataset. A positive MI indicates that the FB registration has a higher MI than Visiopharm's registration. The cores are sorted according to difference in MI. The mean improvement in MI is 0.07 indicated by the red broken line.

APPENDIX D

CD

A CD with the algorithm is only attached in the versions given to the censor and supervisors.

Bibliography

- [1] Breast biopsy,
<http://baysurgicalspecialists.com/breast-biopsies/>.
- [2] Immunohistochemical staining process,
<http://en.wikipedia.org/wiki/File:Immunohistochemicalstaining1.png>.
- [3] Tissue preparation,
<http://www.piercenet.com/browse.cfm?fldid=f95b91a9-3dc1-4b56-8e8d-59ca044a8ba7>.
- [4] Worldwide cancer statistics, <http://www.cancerresearchuk.org/cancer-info/cancerstats/world/cancer-worldwide-the-global-picture>.
- [5] J.M. Fitzpatrick and M. Sonka. *Handbook of Medical Imaging: Medical Image Processing and Analysis*. Handbook of Medical Imaging. SPIE Press, 2000.
- [6] R.C. Gonzalez and R.E. Woods. *Digital image processing*. Addison-Wesley world student series. Addison-Wesley, 2002.
- [7] R. Marone. *The ErbB2 Receptor and Breast Carcinoma Cell Migration: Memo is a Novel Mediator of Cell Motility*. 2003.
- [8] Ivar Skaland, Emiel A M Janssen, Einar Gudlaugsson, Jan Klos, Kjell H Kjellevold, Håvard Søiland, and Jan P A Baak. Phosphohistone h3 expression has much stronger prognostic value than classical prognosticators in invasive lymph node-negative breast cancer patients less than 55 years of age. *Modern Pathology*, 20(12):1307–1315, 2007.

- [9] Georgios Tzimiropoulos, Vasileios Argyriou, Stefanos Zafeiriou, and Tania Stathaki. Robust FFT-Based Scale-Invariant Image Registration with Image Gradients. *IEEE TRANSACTIONS ON PATTERN ANALYSIS AND MACHINE INTELLIGENCE*, 32(10):1899–1906, 2010.